inorganics

MDPI

Review

Inorganic-Based Nanoparticles and Biomaterials as Biocompatible Scaffolds for Regenerative Medicine and Tissue Engineering: Current Advances and Trends of Development

Nabanita Saikia

Department of Chemistry, New Mexico Highlands University, Las Vegas, NM 87701, USA; nsaikia@nmhu.edu

Abstract: Regenerative medicine amalgamates stem cell technology and tissue engineering strategies to replace tissues and organs damaged by injury, aging, ailment, and/or chronic conditions by leveraging the innate self-healing mechanism of the body. The term 'regenerative medicine' was coined by William A. Haseltine during a 1999 conference on Lake Como. Since its inception in 1968, the field has offered clinical benefits for the regeneration, repair, and restoration of bones, skin, cartilage, neural tissue, and the heart, as well as scaffold fabrication. The field of tissue engineering and regenerative medicine can vastly benefit from advancements in nanoscience and technology, particularly in the fabrication and application of inorganic-based nanoparticles and bionanomaterials. Due to the tunable intrinsic properties, i.e., size, topography, surface charge, and chemical stability, inorganic-based nanoparticles and biomaterials have surpassed traditional synthetic materials. Given the wide gamut of near-future applications of inorganic nanoparticles and biomaterials, this article gives an overview of the emerging roles in stem cell regenerative research, tissue engineering, artificial skin and cartilage regeneration, neural nerve injuries, 3D bioprinting, and development of new inorganic bio-scaffolds. The review also addresses the challenges related to the clinical application and tissue compatibility of inorganic nanoparticles and biomaterials, utilizing current state-of-the-art techniques.

Keywords: regenerative medicine; inorganic biomaterials; nanoparticles; tissue engineering; nanotechnology

check for updates

Citation: Saikia, N. Inorganic-Based Nanoparticles and Biomaterials as Biocompatible Scaffolds for Regenerative Medicine and Tissue Engineering: Current Advances and Trends of Development. *Inorganics* **2024**, *12*, 292. https://doi.org/10.3390/inorganics12110292

Academic Editor: Roberto Nisticò

Received: 16 September 2024
Revised: 5 November 2024
Accepted: 6 November 2024
Published: 11 November 2024

Copyright: © 2024 by the author. Licensee MDPI, Basel, Switzerland. This article is an open access article distributed under the terms and conditions of the Creative Commons Attribution (CC BY) license (https://creativecommons.org/licenses/by/4.0/).

1. Introduction

Regenerative medicine is an emerging interdisciplinary area focused on developing methods to replace or repair damaged cells and restore tissue or organ function affected by trauma, chronic conditions, disease, aging, or congenital deformities [1,2]. Regenerative medicine amalgamates the principles of chemistry, biology, and applied engineering to develop processes and therapies that can promote the regeneration of human cells, functional organs, and injured tissues to restore normal body functions [3,4]. By harnessing the human body's innate ability to self-heal, regenerative medicine is poised to revolutionize science, healthcare, and medicine [1]. Regenerative medicine is also used synonymously with 'tissue engineering', which relies on developing scaffolds that can mimic the extracellular matrix (ECM) of tissues [5]. Examples of regenerative medicine include stem cell-based therapy, immunomodulation therapy, and tissue engineering [6]. Tissue engineering is the application of principles and methods of engineering and life sciences toward the fundamental understanding of structure–function relationships in normal and pathological mammalian tissues and the development of biological substitutes to restore, maintain, or improve tissue function [7,8]. The primal goal of tissue engineering is the regeneration of patients' tissues and organs devoid of poor biocompatibility, functionality, and immune rejection [9].

In tissue engineering, cells, scaffolds, and growth factors are crucial for promoting the regeneration of bone and cartilage [10]. Cells synthesize the matrix for the growth

of new tissues [9]. Scaffold materials, templates, or artificial extracellular matrices serve as substrates for loading cells and growth factors, which stimulate cell proliferation, differentiation, biosynthesis, and regeneration [10]. Growth factors are signaling molecules that guide cell behavior to stimulate the growth of new tissues and provide chemical cues to stem cells, regulating their biological responses and tissue differentiation [9,11]. Tissue engineering takes place in the presence of a scaffold which serves as a template for regeneration. Bone tissue engineering and enhancement of bone healing for orthopedic, craniofacial, and periodontal applications can be achieved by a group of multi-functional growth factors called bone morphogenetic proteins (BMPs) [12]. BMPs are members of the transforming growth factor beta (TGFβ) superfamily of cell regulatory proteins that control osteoblastogenesis, embryonic development, cellular function, differentiation, proliferation, morphogenesis, and apoptosis [13]. A signal transduction cascade is initiated upon BMP ligand binding to a transmembrane, heterotetrametric receptor complex composed of type I BMP receptors (BMPR) (ACVR1/ALK2, BMPR1A/ALK3, and BMPR1B/ALK6) and type II BMPR (BMPR2, ActR-2A and ActR-2B) [14,15].

Stem cells are undifferentiated, non-specialized cells that can self-renew and differentiate into other cell types such as liver cells, nerve cells, and cardiomyocytes [3,16,17]. Stem cells are categorized into embryonic stem cells (ESCs), adult stem cells (ASCs), and induced pluripotent stem cells (iPSCs) [18,19]. ASCs include mesenchymal stem cells (MSCs), myogenic stem cells, neural stem cells, and umbilical cord stem cells [20]. ESCs and iPSCs have high self-regeneration ability and differentiation potential [21–23]. Stem cells can be classified based on their ability to differentiate into various cell types [24,25]. The classifications are as follows:

- Totipotent: stem cells can develop into any cell type, including embryonic and adult lineages.
- Pluripotent: stem cells can become any cell type in an adult.
- Multipotent: stem cells can differentiate into multiple cell types within a specific lineage.
- Unipotent: stem cells are limited to differentiating into just one specific cell type.

A current thrust in regenerative medicine research is in cord blood stem cells that can offer patients the much-needed means to life-saving stem cell transplants [26]. Umbilical cord blood, like bone marrow and peripheral blood collected from the umbilical cord and placenta of healthy newborns, contains a rich source of blood-forming stem cells, which can renew and differentiate into other cell types. Cord blood stem cells find applications in transplants for patients suffering from leukemia, lymphoma, aplastic anemia, multiple myeloma, and immune deficiency disorders, and for people facing difficulty finding matched adult donors [27]. Human umbilical cord blood stem cells, an alternative source of hematopoietic stem cells, have expanded transplant eligibility for patients with neurodegenerative and cardiovascular disorders and hematologic conditions, especially from minority groups (racial and ethnic) across the U.S. and worldwide [28–30]. Umbilical cord blood has advantages over bone marrow because cord blood does not require human leukocyte antigen tissue matching, has less incidence of graft vs. host disease, and may be used in allogeneic cell therapy [31,32]. MSCs are widely used for wound healing due to their abundance, high proliferation rate, multilineage differentiation capacity, and expression of paracrine factors [21]. MSCs hold promise in the regeneration of cardiac tissues for improving cardiac function [33–35]. Despite limitations in treatment modalities, costs involved, and limited success, stem cell-based therapeutic strategies have emerged as a promising new approach to enhancing regenerative wound healing [36–38].

The skin is the largest organ in the human body that is prone to damage, such as wear and tear, bruises, scars, ulcers, burns, wounds (infectious or chronic), and aging, which can compromise its integrity and function [21,39]. Cytokines, chemokines, growth factors, and cell signaling cascades are crucial in maintaining the health, integrity, and epidermal regenerative ability of the skin [21,39–41]. The Wnt (Wingless and INT-1) signal transduction cascade is involved in embryonic development, stem cell function, tissue homoeostatic self-renewal in adult organisms, and skin development through canonical and noncanonical signaling pathways, and is linked to the regulation of cell proliferation,

differentiation, migration, and polarity of stem and cancer stem cells [42–44]. Due to the slow recovery and limited self-healing abilities of human skin, there is limited knowledge about preventing skin degeneration and identifying effective therapies for skin regeneration and rejuvenation [45].

The peripheral nervous system (PNS) consists of a network of 43 pairs of motor and sensory nerves that control the voluntary functions of sensation, movement, and motor coordination. The PNS comprises of three types of cells: neuronal, glial, and stromal. Traumatic and infectious diseases can lead to peripheral nerve damage and long-lasting disability affecting both sensory and motor functions [46]. Recovery from peripheral nerve damage is an intractable challenge for clinical researchers, as it is a complex process typically managed through surgical nerve autografting. However, this method has disadvantages, as it often fails to achieve complete nerve recovery and nerve axon regrowth is inhibited due to the presence of nerve gaps [46]. Stem cells such as adipose-derived stem cells (ADSCs), MSCs—in particular, bone marrow stem cells (BMSCs)—and umbilical cord stem cells (endothelial progenitor cells and hematopoietic stem cells) with high proliferative capabilities are suitable candidates for regenerating neural tissues [47–50]. Stem cell-based therapy in peripheral nerve injury can induce nerve regeneration and axonal remyelination by providing the microenvironment for peripheral nerve regeneration and regulating inflammatory cascade after injury [46,51]. Zeng and Zhang discussed innovative approaches for in vivo gene expression reprogramming in neural regeneration and repair [52]. However, continuous efforts are desirable to develop safe and effective therapies to understand the underlying mechanisms that regulate neuronal regeneration in spinal cord repair.

Inorganic nanoparticles have been at the forefront of research in designing novel biomaterial hybrids for versatile biomedical applications, including, but not limited to, cancer, tumor biomarkers for targeted therapy [53], nervous system repair, nanocarriers for antimicrobial drugs [54], nanoprobes or imaging probes for magnetic resonance imaging (MRI), computed tomography (CT), anti-Stokes shift-based optical imaging [55], and engineering technology [56]. This is attributed to its controllable size and composition, unique physical, mechanical, optical, and electronic properties at the nanoscale level, making them outstanding candidates for biomedical research [55,57,58]. Inorganic-based biomaterials, on the other hand, are of particular interest in rapid hemostasis and wound healing [59], bacterial activity, dental restorations, and skin tissue engineering [60], due to improved biocompatibility, higher bioactivity, promotion of blood coagulation, and ability to release bioactive ions [59,61]. The design and development of inorganic-based biomaterials rely on two components: active chemical components—which include gelatin, chitosan, natural and synthetic polymers—and alginic acid. The active inorganic components primarily include silicates, phosphates, and natural minerals. Inorganic biomaterials are typically hydrophilic or super-hydrophilic, have high surface energy, and can readily absorb water to achieve ultra-rapid hemostasis [59]. Furthermore, tunable magnetic, optical, electronic, biophysical, and biochemical properties, along with biocompatibility [62], endow inorganic-based nanoparticles and biomaterials with prospective applications in regenerative medicine and tissue engineering [63], stem cell differentiation, in-growth tissue integration, in vivo stem cell tracking, and other diverse cellular functions [5,58,64]. Hence, a synergistic approach that combines the best of the two research fields can accelerate scientific advancements in disease treatment and therapy, the development of next-generation cell-based therapeutics, and precision medicine. This review discusses the emergent applications and scalability of inorganic-based biomaterials and nanoparticles as novel bio-scaffolds in stem cell regenerative research, tissue engineering, artificial skin and cartilage regeneration, and neural nerve injury. Although excellent reviews and studies cover developments in tissue engineering and regenerative medicine [7,62,64–66], the primary focus of this review is to highlight current progress in the application of inorganic-based biomaterials and nanoparticles in stem cell regenerative research, tissue engineering, artificial skin and cartilage regeneration, cardiovascular disease, and wound healing. The review also accounts for the challenges in

clinical application and tissue compatibility of inorganic nanoparticles and biomaterials utilizing current state-of-the-art techniques.

2. Inorganic-Based Nanoparticles and Biomaterials as Scaffolds in Regenerative Medicine

Contemporary regenerative medicine strategies employ inorganic-based biomaterial scaffolds that mimic the biological and mechanical features of the ECM, thereby enhancing tissue regeneration and healing [1]. Scaffolding materials constitute the structural basis that, at best, can fully, or in part, mimic the native function of the ECM and help cells adhere, proliferate, and differentiate in vitro and in vivo following implantation [67,68]. The fabrication of bio-based inorganic material scaffolds enables the construction of substitute tissues that are biocompatible, safe, and easily biodegradable, without producing toxic byproducts [69]. Polymeric nanoparticles, lipid-based nanoparticles, and inorganic nanoparticles are widely studied in drug delivery, tissue engineering, and biomedical imaging [70–72] to enhance cell viability and achieve optimal cell-directing capabilities [35,72].

Bone regeneration relies on biomaterials that are osteoconductive (supports bone growth and encourages the ingrowth of surrounding bone) as well as capable of osseointegration (osteointegration or integration into surrounding bone). Inorganic biomaterials such as hydroxyapatite (HAP), HAP/poly(lactic-co-glycolic acid) composites, calcium phosphate-based biomaterials, and polymer/ceramic composites have the potential to be osteoinductive, meaning they can induce ectopic bone formation by instructing the surrounding in vivo environment to form bone [19,68,73,74].

Hasan et al. reviewed the diverse applications of inorganic nanoparticles (magnetic, metallic, metal oxide, and metallic) in tissue engineering [75]. Table 1 summarizes the composition of different inorganic-based nanoparticles and biomaterials along with biocomposite materials reviewed in this study. Inorganic-based nanoparticles and biomaterials can be broadly classified based on the material from which they are synthesized or fabricated: carbon nanomaterials, inorganic nanoparticles, inorganic biomaterials, biomimetic natural biomaterials/biopolymers, and biocomposite materials. Carbon nanomaterials include graphene oxide, reduced graphene oxide, fullerene, fullerol, carbon dot, carbon black, and carbon nanotube. The inorganic nanoparticles can be metals, such as gold or silver nanoparticles, or metal oxides (TiO_2, silica, MgO, Fe_3O_4, alumina, and bioactive glass) and are the most widely expended type of nanoparticles in biomedical fields. Biomimetic materials are classified based on their structure, function, manufacturing process, and molecular characteristics [76]. Biomimetic natural biomaterials and biopolymers are typically biocompatible, biodegradable, non-toxic, and have been shown to improve the pharmacokinetic properties and bioavailability for targeted drug delivery [77]. These biomaterials find applications in robotics, superhydrophobic materials design, self-cleaning materials, adhesives, biomedical, and nanotechnology [76].

Table 1. Classification of inorganic-based nanoparticles and biomaterials based on the chemical composition or structure.

Type	Composition/Structure
Carbon nanomaterial	Graphene oxide (GO) Single-wall carbon nanotube (SWNT) Multi-wall carbon nanotube (MWCNT) Carbon dot, Carbon black (Printex 90) Fullerene (C60) Fullerol [$C60(OH)_n$]

Table 1. *Cont.*

Type	Composition/Structure
Inorganic nanoparticle	Silica-iron oxide (SiO_2-Fe_3O_4) Titanium dioxide (TiO_2), Ti-6Al-4V alloy Manganese dioxide (MnO_2), Manganese silicate (MnS) Titanium dioxide-silica (TiO_2/SiO_2) Magnesium oxide (MgO) Bioactive glass (BG) Si−Ca−P−Mo glass-ceramic (BBGN) Gold (AuNP) Zinc oxide (ZnO)
Inorganic biomaterial	Hydroxyapatite (HAP) Calcium phosphate (CaP) Ceramic
Biomimetic natural biomaterial/biopolymer	Poly (L-lactic acid) (PLLA), Polycaprolactone (PCL) Polyhydroxyalkanoates, Hyaluronic acid (HA) Alginate, Cellulose, Chitosan (CS), Collagen Gelatin, Gelatin nanofiber (GNF) Polydimethylsiloxane (PDMS) Fibroin, Hydrogel, Poly-glutamic acid [$(C_5H_7NO_3)_n$]
Biocomposite material	GO-PCL PLLA/PCL/GNF/AuNP PCL/silk fibroin (PCL/SF) PCL/SF/Au(SiO_2) Polysulphone-modified MWCNT Alginate-nano-silica hydrogel Chitosan hydrogel reinforced HAP nanorod (CS-HAPNr) AuNP-collagen Chitosan-collagen-HAP (Cs/Col/HAP) HAP/poly(lactic-co-glycolic acid)

Figure 1 illustrates a multifaceted approach that combines cell therapy, bioactive materials, and biomolecules or external stimulation to treat musculoskeletal diseases affecting bone and muscle through regenerative medicine.

External stimulation, along with signaling molecules, aptamers, peptides, and growth factors can modulate immune response and promote tissue growth essential in regeneration. External stimuli like light, temperature, ultrasound, topography, magnetic fields, or electrical stimulation can activate intracellular signaling cascades, augment intrinsic tissue cell growth, and mitigate regeneration under natural conditions [78]. Therefore, a synergistic strategy that integrates innovative biomaterials, growth factors, and external stimulation offers a comprehensive approach to tissue engineering, effectively addressing patients' needs for treating musculoskeletal conditions. Nevertheless, to treat musculoskeletal disorders, optimizing the stimuli responsiveness and refining currently available therapeutic methods can leverage the effectiveness of therapeutic approaches.

To enhance the effectiveness of stem cell therapy in treating cardiovascular diseases, Chen et al. [35] incorporated a silica–iron oxide (silica-Fe_3O_4) nanoparticle, a superparamagnetic mesocellular foam to increase cell viability and sustained release of cargo in human MSCs. Alternatively, the higher porosity and surface area of mesoporous silica nanoparticles, metallic oxide nanoparticles, HAPs and titanium dioxide (TiO_2) nanotubes have enabled applications in drug delivery, imaging, osteoblast differentiation, and bone regeneration [79]. Surface coating of superparamagnetic iron oxide nanoparticles with silica was shown to reduce the long-term toxicity effects and improve biocompatibility via enhancement of resistance to lysosomal acidity. The Fe_3O_4/SiO_2 nanoparticles were surface-passivated with amino- and sulfonate-silanes, and toxicity studies were performed on A549 and HeLa cell lines [80]. Lactate dehydrogenase (LDH) assay, which measures cell membrane integrity, showed high levels of membrane damage in bare nanoparticles,

while the nanoparticles that were surface coated showed a marginal increase in LDH levels, suggesting the role of surface passivation on cell viability and membrane damage. TiO_2 nanoparticles have been shown to cause genotoxic effects by inducing oxidative DNA damage, and excessive production of ROS can result in strand breakage after 24 h of exposure [81,82]. Data indicated that a decrease in mitochondrial dehydrogenase activity in human lymphocytes, caused by TiO_2 nanoparticles, could increase oxidative stress in cells and serve as mediators for TiO_2 genotoxicity [83]. Genotoxicity studies performed using a comet assay agreed with cytotoxicity measurements, with bare TiO_2 nanoparticles exhibiting increased DNA damage [81,83].

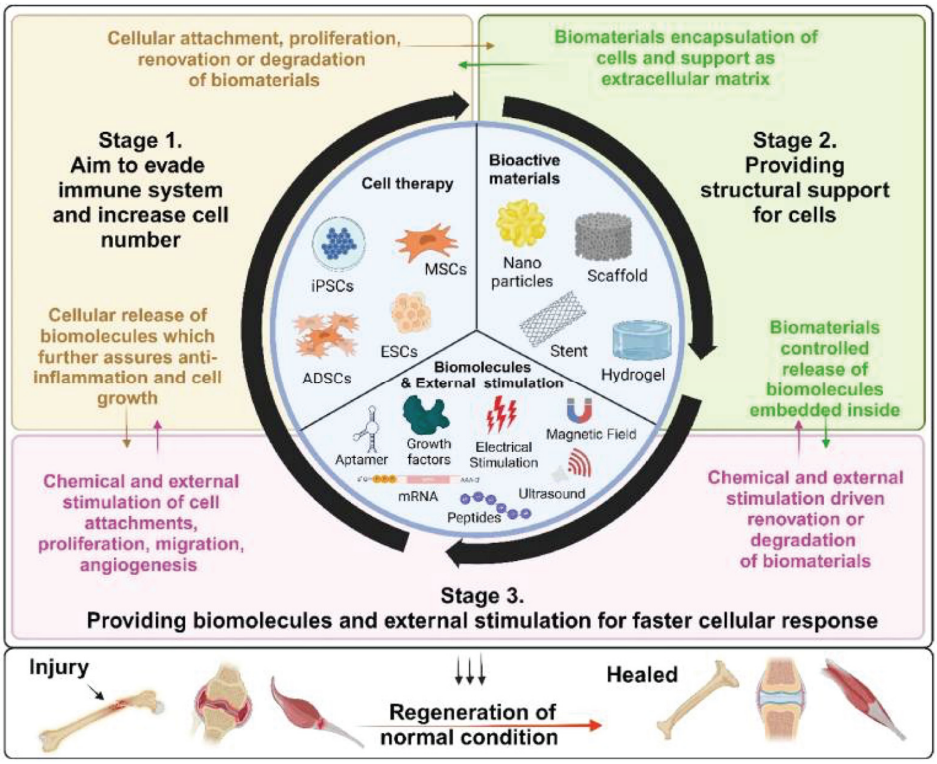


Figure 1. An integrative approach that combines bioactive materials, biomolecules and external stimulation, and cell therapy in musculoskeletal disorders. The figure is reproduced from ref. [78], an open access article under the CC BY-NC-ND license, https://creativecommons.org/licenses/by-nc-nd/4.0/ (accessed on 1 November 2024).

Studies suggested that TiO_2 nanoparticles are prone to accumulation in the alimentary tract, central nervous system, liver, kidney, pulmonary tract, and reproductive system and form agglomerates with other mammalian cells; TiO_2 particles less than 25 nm can accumulate in the spleen, lungs, and kidney while particles of around 80 nm can accumulate in the liver [84]. Since these nanoparticles have the potency to cross the blood–brain barrier, they can induce apoptosis in the hippocampal neurons [84]. TiO_2 nanoparticles of certain sizes can induce oxidative stress, toxic effects, DNA strand breakage, and chromosome damage, leading to elevated expression of inflammatory cytokines and increased occurrence of apoptosis [85]. Studies on LA-9 mouse fibroblast cell lines suggested TiO_2 nanoparticles could induce intracellular ROS production at 150 and 250 μg/mL concentrations after exposure for 24 h [86]. Furthermore, cells exposed to 150 μg/mL concentration exhibited an increased percentage of apoptotic cells when compared to negative control [86]. Cytotoxicity measurements of 3–600 μg/mL of homogeneous and weakly aggregated TiO_2 nanoparticle solution showed variations in cell viability at lower concentrations of TiO_2 (3–6 μg/mL) [87]. Cell viability decreased at concentrations > 6 μg/mL, while cells cultured in 600 μg/mL TiO_2 nanoparticles for 48 h showed a 37% decrease in cell viability [87]. After

48 h of exposure to L929 cell lines, significant cytotoxicity was observed. Higher concentrations of TiO_2 nanoparticles increased oxidative stress, leading to increased ROS and LDH levels, and decreased glutathione (GSH) and superoxide dismutase (SOD) levels [87]. Detailed reviews on the detrimental, hazardous effects of TiO_2 nanoparticles, along with toxicity, can be found elsewhere [83,84,88,89].

Friggeri et al. [90] investigated the potential application of graphene oxide–polycaprolactone (GO-PCL) composite material as a multifunctional 3D-printed scaffold in tissue engineering and medical device design. The composite material exhibited antibacterial and adhesive growth properties, highlighting its potential applications in tissue engineering (Figure 2). PCL and PCL-GO composite of 1 wt.% concentration had low cytotoxicity and did not impair the mechanical properties of PCL. The adsorption of solvent molecules by GO reduced bacterial adhesion during surgical procedures. The cellular adhesion on PCL-GO was significantly lower compared to PCL samples. Biocompatibility analysis was performed with VERO, HEK, C2C12, and RAW cell lines that were plated on PCL and PCL-GO scaffolds, and cell viability after 72 h was measured using the bioluminescence method (Figure 2A). PCL-GO scaffolds had lower cellular adhesion for the cell lines compared to PCL and plastic wells, which were used as controls. The cell adhesion for control was higher than for PCL, as shown in Figure 2A. The reduced cell adhesion of the PCL-GO scaffold was related to PCL's hydrophobicity, which limit intermolecular contacts with the surface. The toxicity profile of VERO cells lines conditioned with PCL-GO scaffolds was observed to be lower than those of cells conditioned with PCL after 7 days of scaffold submersion in DMEM (Dulbecco's Modified Eagle's Medium), as shown in Figure 2B. The decreased cell adhesion in PCL-GO lessened biofouling risks in a surgical environment. Controlling the long-term cell adhesion ensured scaffold biodegradability and population over time, which was vital in promoting successful tissue regeneration. Fluorescence images showed visible dead cells (shown in red) that point to a local cytotoxic effect of PCL-GO along the scaffold borders, as indicated by the arrows (Figure 2C,D). PCL and PCL-GO scaffolds were washed with PBS or PBS + ethanol (Figure 2E), and the number of cells attached to the scaffold increased with the number of washes. PCL-GO scaffold showed a five-fold increase in cell attachment compared to PCL. The bioconductivity of PCL-GO scaffolds reached that of PCL after repeated washing with DMEM medium (Figure 2F). Lastly, fluorescence imaging of VERO cell lines grown on DMEM-washed scaffolds did not show the presence of dead cells along the scaffold borders (Figure 2G,H). The study proposed a low-cost, yet versatile strategy in the application of GO-PCL composite material as a 3D-printed scaffold for developing biomedical implants.

The scaffolding function of poly (L-lactic acid) (PLLA)/PCL composite matrix containing gelatin nanofibers (GNFs) and gold nanoparticles (AuNPs) were studied in bone tissue engineering [91]. The solubility properties, coupled with biocompatibility, biodegradability, and low immunogenicity, make gelatin a suitable biopolymer for tissue engineering applications [92]. Furthermore, the Arg-Gly-Asp (RGD) domains in gelatin promote cell attachment and proliferation. The induced toxicity and cellular proliferation of MG-63 cells on the fabricated scaffolds were measured using MTT and LDH assays [91]. PLLA/PCL/GNF/AuNPs (80 ppm) showed the highest cell growth at 72 h (Figure 3). PLLA/PCL/GNF/AuNPs (160 ppm) at 72 h after cell seeding had lower cell proliferation than control, while test groups showed higher cell proliferation than control.

The rat calvarial defect model was used to evaluate bone healing, and the histomorphometric data is provided in Table 2. The poorest bone regeneration was observed in the negative control group. The defect treated with PLA/PCL/GNF/AuNPs (80 ppm) exhibited the highest fibroblast + fibrocyte, osteoblast + osteocyte, and osteon values, which indicated the highest bone regeneration. The observation of osteoclast cells demonstrated greater bone regeneration than bone resorption; bone regeneration was enhanced in defects treated with PLA/PCL/GNF/AuNPs (80 ppm) [91].

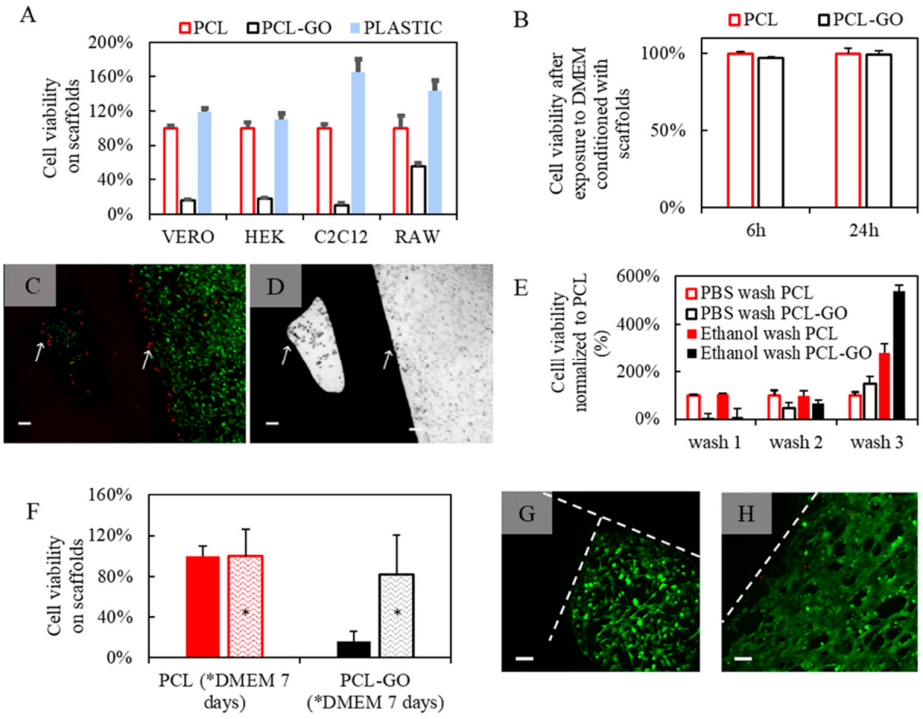


Figure 2. (**A**) Viability of different cell lines grown on scaffolds or plastic wells evaluated using a luminescence assay. (**B**) Toxicity of DMEM exposed to scaffolds for 7 days and used to treat VERO cells seeded on 96-well plates. Toxicity on VERO cells was evaluated after 6 or 24 h of treatment. (**C**) Fluorescence imaging of VERO cells surrounding grids of PCL-GO. Cells have been labeled with calcein (green) to evaluate viable cells and propidium iodide (red) to evaluate dead cells. The brightfield image of the same sample is shown in (**D**). Arrows indicate boundaries between the scaffold and well. (**E**) Evaluation of VERO cell viability on scaffolds washed with PBS or PBS + ethanol. (**F**) Cell viability on the scaffold without DMEM washing and after washing with DMEM, indicated with asterisks (*). (**G**,**H**) Representative fluorescence images of cells surrounding grids (dashed lines) after DMEM washings; no red dead cells were visible. The scale bar is 100 µm. The figure and caption are reproduced from ref. [90]. Copyright © 2024, G. Friggeri, I. Moretti, F. Amato, A. G. Marrani, F. Sciandra, S. G. Colombarolli, A. Vitali, S. Viscuso, A. Augello, L. Cui, G. Perini, M. De Spirito, M. Papi, V. Palmieri. This article is distributed under a Creative Commons Attribution (CC BY) license, http://creativecommons.org/licenses/by/4.0/ (accessed on 1 November 2024).

Table 2. Histomorphometric analysis of bone tissue regeneration in the defects treated with PLA/PCL/GNF, PLA/PCL/GNF/AuNPs (40 ppm), PLA/PCL/GNF/AuNPs (80 ppm), and PLA/PCL/GNF/AuNPs (160 ppm). Reproduced from ref. [91].

	Negative Control	**PLA/PCL/GNF**	**PLA/PCL/GNF/AuNPs**		
			40 ppm	**80 ppm**	**160 ppm**
Fibroblast + fibrocyte	62.10 ± 3.55	79.42 ± 18.64	93.90 ± 16.03	109.11 ± 22.45	87.09 ± 13.10
Chondroblast + chondrocyte	102.40 ± 5.44	88.50 ± 11.37	53.73 ± 6.74	55.26 ± 4.99	67.32 ± 7.88
Osteoblast + osteocyte	23.25 ± 4.65	51.25 ± 18.09	85.34 ± 16.22	97.60 ± 27.16	76.31 ± 15.05
Osteoclast	3.78 ± 1.66	4.54 ± 1.09	3.31 ± 2.14	2.65 ± 1.28	4.21 ± 0.98
Osteon	3.67 ± 1.27	5.57 ± 1.99	6.93 ± 2.44	7.55 ± 1.69	4.50 ± 1.08

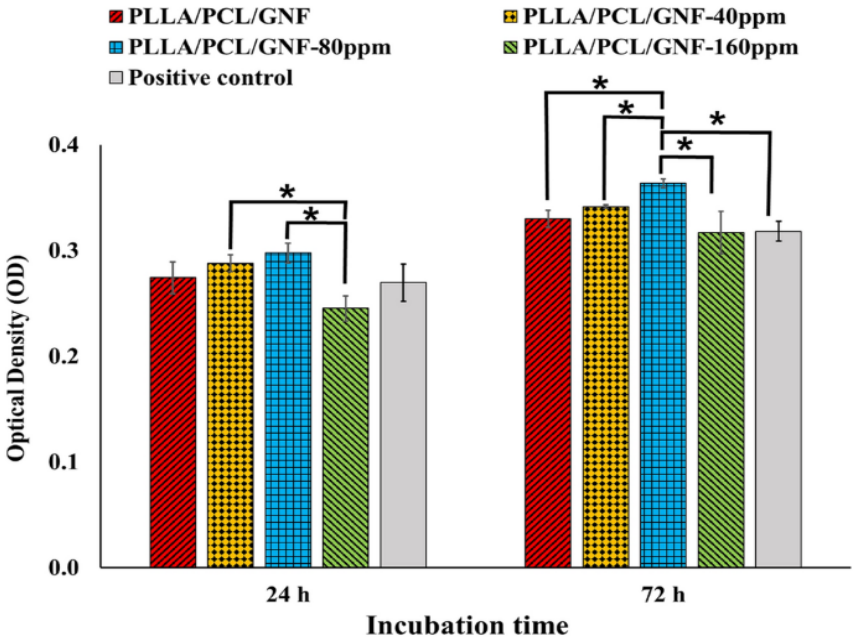


Figure 3. MG-63 cell proliferation on the fabricated scaffolds was measured using an MTT assay at 24 and 72 h after cell seeding. Control: Tissue Culture Plate (TCP). Data represented as mean ± SD, $n = 3$. * $p < 0.05$ (obtained by one-way ANOVA). The Figure is reproduced from ref. [91]. This article is licensed under a Creative Commons Attribution 4.0 International License, http://creativecommons.org/licenses/by/4.0/ (accessed on 1 November 2024).

The in vivo data indicated defects treated with PLA/PCL/GNF/AuNPs (80 ppm) induced higher neo-bone formation. AuNPs (80 ppm) incorporated in the scaffolds did not interrupt the normal functioning of cells. PLA/PCL/GNF/AuNP (80 ppm) scaffold induced the highest bone regeneration, and the incorporation of AuNPs and GNFs mimicked the native structure of bone and stimulated bone healing.

Nanofibrous composite scaffolds of PCL, PCL/silk fibroin (SF), and PCL/SF/Au(SiO_2) were fabricated to study bone tissue regeneration of human MSCs (hMSCs) [93]. The nanofibrous scaffolds had high porosity and exhibited a uniformly connected fibrous structure with polydispersed Au(SiO_2) nanoparticles on the scaffold surface. Table 3 shows the fiber diameter, pore size, % porosity, and tensile strength of PCL, PCL/SF, and PCL/SF/Au(SiO_2) electrospun nanofibrous scaffolds.

Table 3. Characterization of nanofibrous scaffolds of PCL, PCL/SF, and PCL/SF/Au(SiO_2). Reproduced from ref. [93].

Nanofibrous Constructs	Fiber Diameter (nm)	Pore Size (μm)	Porosity (%)	Tensile Strength (MPa)
PCL	215 ± 32.12	1.45 ± 0.26	88 ± 4.3	7.63
PCL/SF	164 ± 18.65	2.12 ± 0.31	92 ± 6.3	11.67
PCL/SF/Au(SiO_2)	172 ± 24.22	2.35 ±0.22	90 ± 7.5	12.11

The scaffolds have a fiber diameter in the range of 164 ± 18.65 to 215 ± 32.12 nm, as shown in Table 3. The pore sizes of PCL, PCL/SF, and PCL/SF/Au(SiO_2) are 1.45, 2.12, and 2.35 μm, respectively. The porosity values of PCL, PCL/SF, and PCL/SF/Au(SiO_2) scaffolds are 88 ± 4.3%, 92 ± 6.3%, and 90 ± 7.5%, respectively, which are within the desirable range for bone tissue regeneration. The porosity of 88% in PCL was below the optimal requirement of 90%. Inclusion of Au(SiO_2) to the scaffold led to increased porosity, as shown in Table 3. Cell proliferation studies of hMSCs on TCP, PCL, PCL/SF, and PCL/SF/Au(SiO_2) nanofibrous scaffolds on days 7, 14, and 21 suggested that hMSCs grown on PCL had a lower proliferation level than PCL/SF and PCL/SF/Au(SiO_2), which

was attributed to the absence of active binding sites in PCL. The higher proliferation level ($p < 0.05$) for PCL/SF and PCL/SF/Au(SiO_2) scaffolds contributed to the bioactive SF and Au(SiO_2) that increased the hydrophilicity essential for cell adhesion [93]. The Au(SiO_2) stimulated cell growth and tissue formation, while SF and Au(SiO_2) stimulated the proliferation of hMSCs without inducing any toxicity.

Composite membranes based on polysulphone-modified multi-walled carbon nanotubes and short carbon fibers were synthesized to elucidate the physicochemical, mechanical, and biological properties [94]. The in vitro results indicated that the membranes were biocompatible when in contact with MG-63 cells. The interaction mechanism between the cells and the composites was influenced by the porosity of the membranes, the presence of carbon additives on the membrane surface, and surface chemistry. Sithole et al. [95] developed a novel 3D-printed biomaterial scaffold to guide host cell growth for bone tissue regeneration. To investigate the potential for bone tissue regeneration/formation, 3D-printed scaffolds were implanted in nasal bone defects of New Zealand white rabbits. Osteoblast-like MG63 cells were used to culture the 3D printed scaffold for 1, 3, and 7 days, respectively. The energy-dispersive X-ray (EDX) analysis showed the presence of Cl, Ca, Na, Si, and P in the mineralized 3D-printed biomaterial scaffold immersed in simulated fluid (SBF) at pH 7.4 for 7 days. On the other hand, the EDX analysis of non-mineralized control scaffold showed the presence of Na, Si, and Cl. This indicated that the biomineral scaffolds had essential biomineralization capabilities crucial for biological growth. The scanning electron microscopy (SEM) images of osteoblast-like MG63 cell adhesion onto 3D-printed biomaterial scaffolds and the scaffold without cells (control) is depicted in Figure 4. The MG63 cells were successfully seeded onto the 3D-printed scaffold, and the rough surface was suitable for cell adhesion to the surface of the implanted devices. In vitro release kinetics experiments were performed to elucidate the performance of the biomaterial scaffold and evaluate the release of BMP-7 protein/growth factor from the biomaterial scaffold in a way that mimicked natural bone fracture healing [95]. For this, the scaffold was loaded with 40.45 ng/mL of BMP-7, and a BMP-7 ELISA Kit was used to study the release profile. BMP-7 was found to adhere to the biomaterial scaffolds surface leading to early burst release. Cell viability measurements further supported the biocompatibility of 3D-printed biomaterial scaffolds, as osteoblast-like MG63 cells were observed to be viable for 7 days.

A biodegradable nanochannel (BNC) membrane was developed through hierarchical cell assembly of 3D manganese dioxide (MnO_2) nanostructures for applications in tissue engineering, cell assembly, and disease modeling, featuring rapid and controllable degradation under biological conditions [96]. As discussed in this study, rapid biodegradation rates of one to three orders of magnitude higher than current polymeric materials make MnO_2 a desirable nanomaterial for membrane construction. The BNC membrane enabled the generation of robust scaffold-free cell sheets and provided a versatile cell assembly-based approach. The cell patterning was visualized using two cell lines labeled with green fluorescence protein (GFP, Cell A) and red fluorescence protein (RFP, Cell B). A densely packed "core–shell" co-assembly of Cells A and B was observed with Cell A surrounded by Cell B, confirming high precision in the patterning process. To recapitulate chronic inflammation in the human skin wound healing process, multicellular patterning of human monocyte-derived macrophages and human fibroblasts was carried out using BNC membrane, placed on a bio-inert cellulose membrane to prevent the tissue from folding. The migration rate of fibroblasts was much slower ($\approx$1 mm/day) compared to conventional scratch assays. The BNC membrane was shown to be suitable in murine diabetic wound healing and chronic skin inflammation. Both in vivo models and in vitro experiments demonstrated the therapeutic efficacy of the BNC cell assembly technique for heterogeneous cell patterning across various cell types. This study by Yang et al. [96] demonstrated a proof-of-concept application of BNC membrane-based 3D cell sheet assembly, achieved in a scaffold-free manner, which is suitable for treating wound healing.

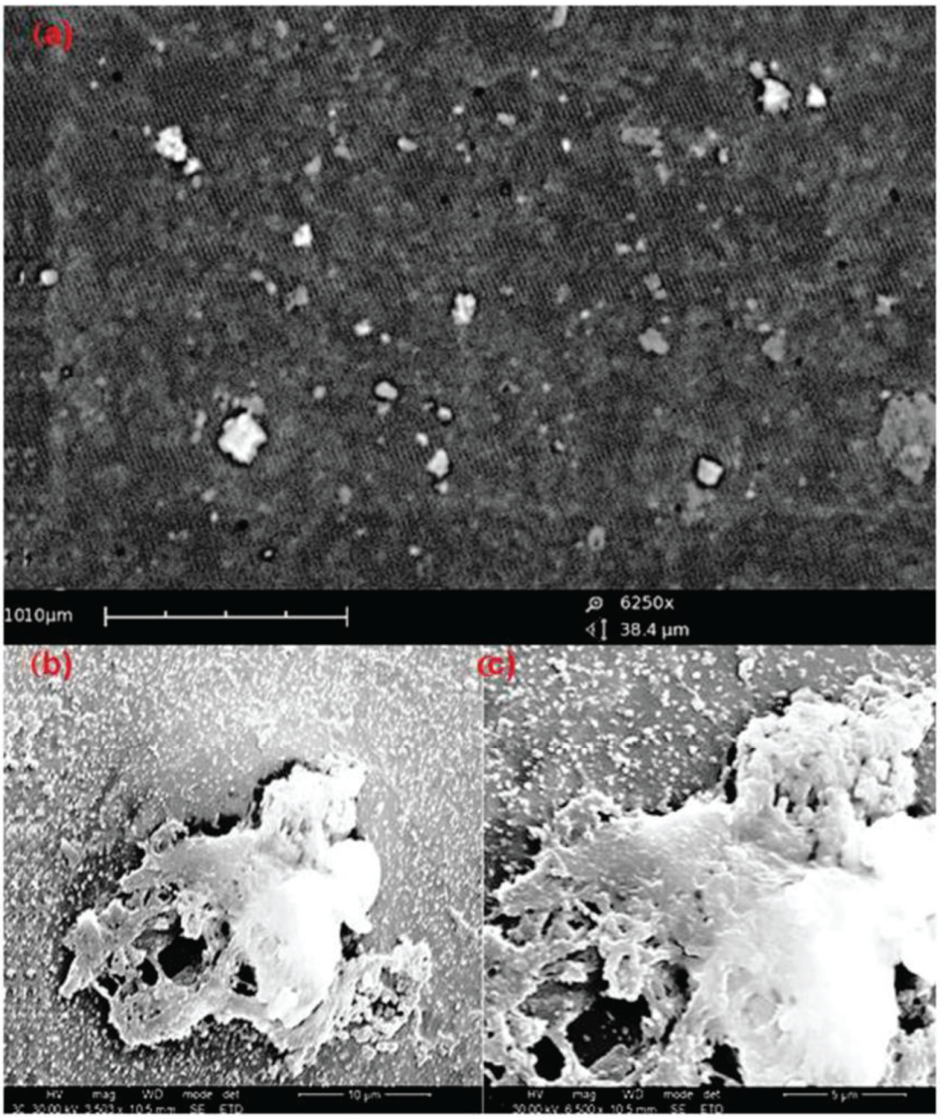


Figure 4. The SEM images on 3D-printed biomaterial scaffolds seeded with osteoblast-like MG-63 cells and the scaffold without cells (control). (**a**) Reference scaffold or scaffold without the cells, (**b**) day 7 cell adhered on the surface of the printed scaffold, (**c**) magnified image of day 7 of cell adhered to the printed scaffold surface. Reprinted with permission from ref. [95]. This article is an open access article distributed under the terms and conditions of the Creative Commons Attribution (CC BY) license, https://creativecommons.org/licenses/by/4.0/ (accessed on 1 November 2024).

To improve the selective differentiation and transplantation of human patient-derived neural stem cells (NSCs), Yang et al. [97] developed a 3D biodegradable hybrid inorganic (BHI) nanoscaffold for stem cell-based tissue engineering and therapy. A biodegradable MnO_2 hybrid scaffold was fabricated, and the interaction of 2D MnO_2 nanosheets with laminin, an ECM protein was investigated. Laminin exhibited a 7.5-fold increase in adsorption on MnO_2 compared to glass (control) and polymer substrates. This was attributed to the polar-π and electrostatic interactions between the biomolecules and MnO_2 nanosheets. The neuronal differentiation of stem cells using MnO_2 was studied using human-induced pluripotent stem cell (hiPSC)-derived NSCs as a model system. A 43% increase in neuronal differentiation and 11-fold increase in neurite outgrowth was observed, due to improved laminin binding and focal adhesion-related pathways. This study validated the potential of hybrid MnO_2 nanoscaffold in improving stem cell survival and inducing neuronal differentiation in vivo.

3. Nanotechnology Strategies in Regenerative Medicine and Wound Healing

The application of nanotechnology in tissue engineering and stem cell biology has fostered new frontiers in research [98]. The novel design principles and characterization techniques, coupled with tunable intrinsic properties and functional specificity, can stimulate the integration of nanomaterials in regenerative medicine therapies [66]. A basic understanding of cell topography is crucial, particularly in terms of how the surrounding environment influences cellular behavior. This includes insights into physical interactions such as cell adhesion, proliferation with scaffold materials, and differentiation. These factors play a significant role in regulating signaling behavior and cellular fate [66,99]. Brovkina and Dashinimaev reviewed regenerative medicine approaches in diabetes mellitus [100]. Li et al. [101] reviewed the application of nanotechnology (nanomedicine, nanomedicine carriers, nanocontrast agents, and nanosensors) in diabetes management and diabetic regenerative medicine. Nanomaterial scaffolds that mimic the natural ECM enhance cell–scaffold interactions, promote the formation of implanted/transplanted tissue-like structures, and facilitate adhesion, oxygen exchange, and nutrient transport [101]. In the treatment of diabetes, nanoparticles were shown to protect insulin from degradation within the gastrointestinal environment and modulate insulin release in response to changes in glucose concentration [102–104]. Polymeric nanoparticles, liposomes, and lipid nanoparticles are the main types of nanoparticles employed in diabetes treatment [70]. These nanoparticles can deliver drugs to the target site, cross the intestinal epithelial barrier while shielding the drugs from environmental conditions, increase drug adsorption, and improve receptor-mediated endocytosis [105,106]. The application of inorganic nanoparticles and polymer nanocomposite materials in early diagnosis and diabetes regenerative medicine has been reviewed elsewhere [102,107–109].

3.1. Engineered Nanomaterials

Engineered nanomaterials or precisely engineered nano–bio interfaces can mimic the natural ECM and facilitate stem cell proliferation, migration, and differentiation into desired cell types [110,111], bone and cartilage repair, and nerve regeneration [111–113]. At the molecular level, engineered nanomaterials can be tailored by modulating the surface properties to provide localized, sustained release of biological molecules and increase therapeutic efficacy [114]. Przekora reviewed the application of engineered biomaterials in bone and cartilage regeneration for long-lasting antimicrobial protection [115]. Wu et al. developed nanotopography patterns in the forms of nano pillars, -holes, and -grills on polycarbonate surfaces to study their effects on human MSC chondrogenesis [116]. Using nanoimprinting technique, nanopillar, nanohole, and nanogrill patterns were constructed to provide topological cues in cartilage collagen fibril orientation. The nanotopographies were patterned on PCL film, and chondroitin sulfate was immobilized on the surface to provide a chondro-inductive biochemical cue for MSC chondrogenesis [117,118]. MSCs on nanogrill and non-patterned surfaces showed an increased cell proliferation rate with a significantly higher DNA amount at day 14 compared to day 1. The initial proliferation on the nanogrill was similar to the that of the non-patterned surface but stopped by day 14. Comparatively, MSCs on nanopillar and nanohole surfaces underwent negligible proliferation; the DNA amount throughout the culture period was not significantly higher than at day 1. The different nanopatterned topography affected the proliferation profile of MSCs. Significantly higher upregulation of hyaline chondrogenic markers and type II collagen was detected on nanopillar and nanohole surfaces, while the expression of this marker was delayed and was at lower levels on the nanogrill surface. This study demonstrated the effect of nano-topography on MSC chondrogenic differentiation; the nanotopographical pattern triggered changes in MSC morphology and cytoskeletal structure, thereby affecting cell aggregation and differentiation.

Atomic layer deposition (ALD) is a cutting-edge nanofabrication technique used in engineering nano-bio interfaces, understanding nano–bio interactions, and developing defect-free and pinhole-free hetero-structured sensing electrodes and layered nanofilms [119,120].

ALD mediates the deposition of thin films on the surface of substrates to form a homogenous coating [121,122]. Bechelany et al. [121] reviewed the synthesis of nanostructured materials using the ALD method for applications in sensing (using nanopore technology) and gas separation membrane technology in water treatment. Pure titanium and Ti-6Al-4V alloy are two biomedical implants widely used in dental and orthopedic applications due to their biocompatibility, superior mechanical properties, and corrosion resistance. However, these implant materials suffer wear and tribocorrosion that releases ions and metallic particles, causing implant loosening and loss in stability [123,124]. TiO_2 coating using ALD improved the mechanical properties, interfacial biocompatibility, water resistance, and cell adherence for high cell–surface interactions [125]. Capek et al. [125] investigated the cellular response of nanotubular oxides of Ti and Ti-6Al-4V alloy to improve cell growth on implants using the ALD technique. Surfaces with ultrathin 1c TiO_2 ALD coatings had a thickness of 0.055 nm and did not result in any morphological changes. Cell proliferation studies of MG-63 cells on ALD-coated Ti-6Al-4V foils showed the growth of elongated MG-63 cells on AM-TiAlV coated with 1c TiO_2 ALD in comparison with uncoated AM-TiAlV by approximately 15%. After 48 h and 72 h, a 2.5-fold and 4-fold increase in the number of cells cultured on AM-TiAlV + 1c TiO_2 was observed. The increased cell proliferation on 1c TiO_2 ALD coating was attributed to the chemistry of the surface and wettability whereby the ultrathin TiO_2 coating lessened the negative cytotoxicity effect of poisonous elements, such as F and V, in biomedical Ti-6Al-4V alloys.

ALD at low temperatures improved the mechanical durability, wetting, and optical properties of TiO_2/SiO_2 nanoparticle films on glass and polycarbonate substrates with precise control of thickness [126]. ALD was utilized for conformal coating of Al_2O_3 oxide thin films, which is a well-defined ALD system on TiO_2/SiO_2 nanoparticle layer-by-layer (LbL) films as a function of ALD-cycle number. The surface morphology of LbL films was not affected by the ALD (thickness of ~1 nm) compared to ~22 nm for silica nanoparticles used as the outermost layer. The contact angle of water on TiO_2/SiO_2 films on glass increased with the number of ALD cycles, and impurity levels were ~0.1–1 atom %. The superhydrophilicity (contact angle < 5°) was restored in the films, and the films were superhydrophilic even after 30 days. Priming polycarbonate substrates with Al_2O_3 ALD coatings before LbL assembly significantly improved the uniformity of TiO_2/SiO_2 films, and ALD-deposited Al_2O_3 showed a surface potential of 20.6 $\pm$ 4 mV.

ALD was used for the uniform coating of nanostructured TiO_2 on commercial Ti substrates using tetrakis(dimethylamino)titanium in combination with H_2O or ozone as an oxidant [125]. The ALD-coated Ti-TiO_2 sample thin films were studied on three different types of bacteria (gram-positive, gram-negative, and antibiotic-resistant). In vitro bacterial results indicated that Ti-TiO_2 at 160 °C significantly inhibited the adhesion and growth of *S. aureus*, *E. coli*, and MRSA bacteria (exceeding 80%) compared to Ti control. The osteoblast adhesion on Ti-TiO_2 samples was significantly higher than Ti control after 4 h of culture. The enhanced adhesion and proliferation of osteoblast cells were facilitated by the increased surface roughness and surface energy of the TiO_2-coated samples, which promoted cell–surface interactions between the osteoblasts and the surface [125].

Room-temperature ALD technique was used to coat collagen membranes with MgO [127] for improved osteointegration. This method enhanced the biocompatibility of collagen and allowed for the deposition of ultra-thin layers of metal oxides that featured uniform thickness and composition, ensuring a conformal, pinhole-free coating [128]. SEM micrographs of uncoated collagen (Col), collagen after 200 ALD cycles of MgO (Col-MgO200), and collagen after 500 ALD cycles of MgO (Col-MgO500) showed regular patterns on the Col-MgO500 sample. As the number of ALD cycles increased, collagen fibers became thicker, and striations in the individual fibers were no longer visible on the coated samples. Atomic force microscopy demonstrated a wavy topography of the samples due to the fibrous and wavy topography of the collagen membrane. The MgO-coated collagen membrane was non-toxic to human cells, displayed improved antimicrobial activity against bacterial biofilms, and facilitated the controlled release of Mg ions [128]. ALD was used

for coating commercially obtained nanoporous alumina membranes with platinum or zinc oxide [129]. An ALD of 8 nm of platinum was coated onto a 20 nm pore size nanoporous alumina membrane, which had high porosity and monodispersed pore size. The pores of PEGylated platinum-coated nanoporous alumina membranes were free of fouling. No protein adsorption, fibrin networks, or platelet aggregation were observed on the membrane surface, suggesting that ALD can serve as a scalable, cost-effective method.

3.2. Carbon Nanomaterials

The design and application of carbon nanotube-based nano–electron mechanical systems (NEMS) in medical nanorobots was reviewed by Popov et al. [130]. Carbon nanotube-based NEMS actuation was achieved using a nanomanipulator, an electric field acting on encapsulated ions, and a magnetic field acting on the magnetic core of the piston. The movable core of the nanotube's wall was polarized by the electric field [130]. The electric field could move metal atoms within the nanotube, transforming them into ions. Wang et al. [131] fabricated 3D carbon nanotube-based composite scaffolds for applications in cartilage repair and tissue engineering. The structure and morphology of carboxylated single-walled carbon nanotube (SWNT-COOH) composite scaffolds were characterized using SEM. The pore size and compression strength of the composite scaffold was modulated by changing the SWNT-COOH concentration. The compression strength increased, while the size of the pore opening decreased with increasing weight percent of SWNT-COOHs. The BMSC proliferation on the composite scaffold suggested that at 7 days, the number of BMSCs in the 2.0 wt. % group was significantly higher than in the 0, 0.5, and 1.0 wt. % groups. However, there was no obvious difference in the number of BMSCs between the three groups. The restorative effects of SWNT-COOH scaffolds were studied using a rabbit model of articular cartilage defects (Figure 5).

In the control group, the cartilage defects were hollow, and reddish granulation tissue at the bottom surface of defects was observed 4 weeks after implantation. The 0 wt. %, 0.5 wt. %, 1.0 wt. %, and 2.0 wt. % groups suggested better filling of defects with no degradation in the composite scaffolds. Repair of cartilage defects was enhanced at 8 weeks after implantation, and the hollows in the control group reduced by half. Except for the control and 2.0 wt. % groups, cartilage defects were fully replaced with repaired tissue at 12 weeks. The cartilage defects in the 0 wt. % group were filled with regenerative cartilage, as shown in Figure 5D. The defects were covered with a smooth, white, semi-transparent cartilage in the 0.5 wt. % group, indicating that this group was superior in repairing cartilage defects.

The chondrogenic potential of multi-walled carbon nanotubes (MWCNT) and hyaluronic acid (HA) was investigated for 3D bioprinting of cartilage constructs [132]. A live/dead assay was performed on the bio-printed constructs after 1 day, 14 days, and 21 days to determine the viability of hMSC-AT cells in the 3D scaffolds. HA-enriched constructs showed a decline in cell viability. The control medium also showed a constant decrease in cell viability, while the differentiation medium exhibited a profound decline in cell viability, despite having the highest transcriptional activity. The MWCNT constructs did not show any decline in cell viability, indicating its protective effect on cells. This was due to the resemblance of CNT to collagen fibrils, which had a stimulating effect on the cells. Scaffolds supplemented with MWCNTs and HA showed the highest cell viability. MWCNTs had a favorable influence on cell viability, while the inclusion of HA had a negative impact on the integrity of constructs. Live/dead analysis indicated that the viability of cells decreased over time for scaffolds without additives (control and differentiation medium), and with HA.

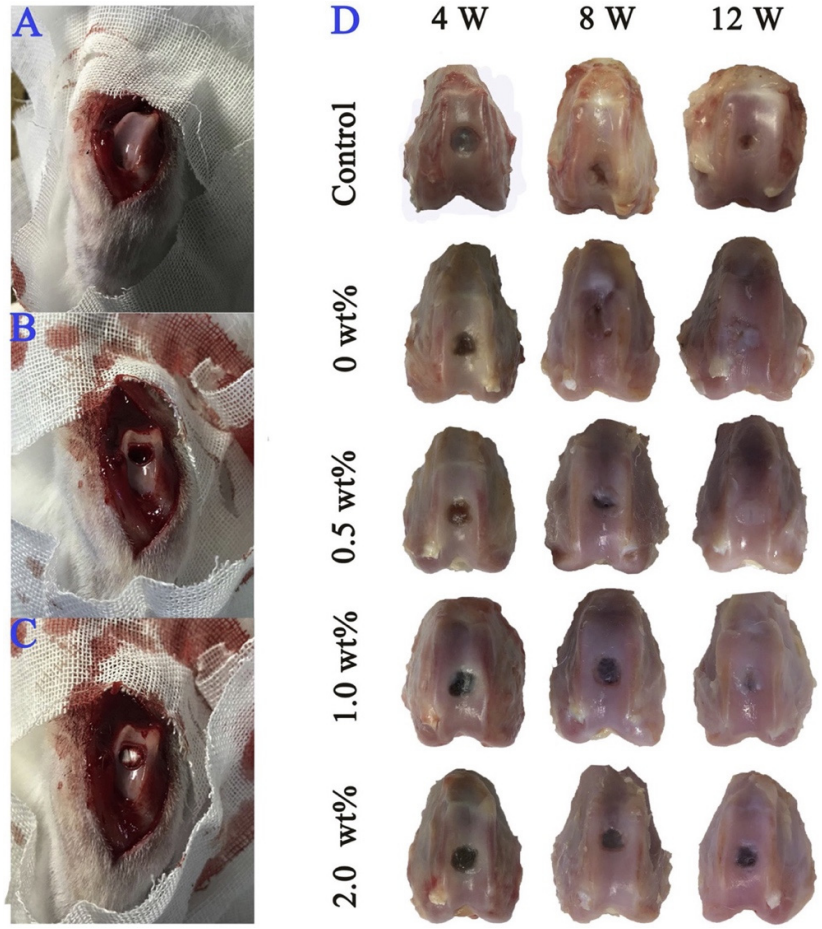


Figure 5. A rabbit model depicting articular cartilage defects and gross observation of defects in the allotted time after operation. (**A**) Smooth and glossy surface of normal articular cartilage. (**B**) Rabbit model of articular cartilage defects. (**C**) Rabbit model of articular cartilage defects filled with composite scaffolds. (**D**) Cartilage defects in control, 0 wt. %, 0.5 wt. %, 1.0 wt. %, and 2.0 wt. % groups at 4 weeks, 8 weeks, and 12 weeks of implantation. Reprinted with permission from ref. [131] from Elsevier.

Polyhydroxylated fullerene (fullerol) was studied for the osteogenic differentiation of human ADSCs and the effect of fullerol on osteogenic differentiation was determined independently and in osteogenic medium [133]. The expression of osteogenic markers was elevated in the presence of a high dose of fullerol. Fullerol inhibited the expression of adipogenic and osteogenic markers in a mouse bone marrow stromal cell line. Fullerol was shown to be nontoxic toward human ADSCs at doses up to 10 μM. Pre-treatment and co-treatment of fullerol enhanced the osteogenic capacity of human ADSCs in culture, and fullerol stimulated gene expression of FoxO1 and its target genes Runx2 and SOD2. As osteogenesis and adipogenesis are regarded to be closely correlated with the capacity of the progenitor cells during bone regeneration, fullerol was shown to inhibit the differentiation of marrow stromal cells and OP9 preadipocytes into adipocytes due to its scavenging activity against intracellular ROS. This study suggested that fullerol could serve as a novel pharmaceutical candidate to produce augmented bone regeneration.

CNT-coated and textured polydimethylsiloxane (PDMS) scaffolds were studied to support the growth of chondrocytes–cells that produce and maintain cartilage [134]. The COOH functionalization led to improved cell adhesion. In this study, four different scaffold architectures, namely, flat (F) and textured (T) PDMS (F-PDMS and T-PDMS), were coated with MWCNT-COOH (F-PDMS-MWCNT and T-PDMS-MWCNT). The addition of MWCNTs atop PDMS produced an isotropic fibrous architecture and enhanced rough-

ness that mimicked the structure in native cartilage. The chondrocytes were observed to form clusters that reduced cellular contact with the substrate. The nano-level roughness increased by ~270% and cell adhesion improved with the addition of MWCNT coating on PDMS scaffolds.

Graphene oxide (GO) and reduced graphene oxide (rGO) mats were examined for their potential to induce neuronic differentiation of ADSCs, which can serve as alternatives to MSCs, demonstrating their ability to differentiate into neuron-like cells [135]. The study demonstrated that graphene nanomaterial-based mats served as suitable stem cell culture platforms for the neurogenic differentiation of ADSCs and GO accelerated the differentiation of ADSCs into neuron-like cells. Neuron-like cells displayed typical neuronal morphology, and the growth, proliferation, and neurogenic differentiation rates of ADSCs seeded on GO mats were superior to those on other substrates.

PCL-based nanocomposite scaffolds with GO nanoshells and two osteogenic drugs, dexamethasone and simvastatin (PCL/GO-Dex and PCL/GO-Sim), were fabricated to examine the osteogenic differentiation, cell viability, and biomineralization on MSCs [136]. The dexamethasone releases from PCL/Dex and PCL/GO-Dex were 69.61 and 49.97%, while the simvastatin releases from PCL/Sim and PCL/GO-Sim were 84.02 and 99.27%, respectively. The presence of GO nanosheets led to less drug being encapsulated in scaffolds, which may be due to the π-π stacking interactions between the drug and GO. PCL/GO-Dex nanocomposite had a higher ability to induce differentiation of MSCs to bone cells. While cell viability increased on PCL/GO and PCL/Dex scaffolds compared to PCL after 7 days, there was no significant change observed after 14 days.

Protein and protease inhibitors were synthesized to improve the therapeutic efficacy of carbon nanofiber-based scaffolds in chronic wound fractures, bone defect repair, and bone marrow-induced inflammation prevention [137]. The nanofibers exhibited superior biocompatibility, cell adhesion, and cell proliferation, and the C-reactive protein was released continuously from the nanofibers for more than four weeks. Doxycycline drug loading of 10% and 15% was considered to investigate the release behavior from the nanoscaffold [137]. For 10% doxycycline drug loading, carbon nanofibers containing only doxycycline released 24% of doxycycline after two weeks of culture. The dual drug nanofibers released 5% of doxycycline when the drug loading of doxycycline was 15%. An increase in doxycycline drug loading from 10 to 15% increased the release rate from the dual drug nanofibers. This was correlated to changes in the hydrophilic properties of the fibers. Shen et al. [138] reported the inhibitory effect of carbon black (Printex 90) on the osteogenesis of bone marrow-derived MSCs and the role of mitochondria in carbon black Printex 90-induced suppression of MSC osteogenesis. Printex 90 dosage of 0.03 μg/mL or below had no detrimental effect on cell viability. For osteogenic differentiation, Printex 90 was added to the osteogenic induction medium, replacing the regular culture medium once MSCs seeded in the culture plates reached 60% confluence [138]. Printex 90 caused a downregulation of osteoblastic markers, reduced the activity of alkaline phosphatase (ALP), and led to poor mineralization of osteogenically induced MSCs.

It is well established that pristine carbon nanomaterials such as carbon nanotubes and graphene-based materials are cytotoxic due to their poor biocompatibility, low solubility in aqueous solvents, and inherent hydrophobicity. Surface functionalization via covalent and noncovalent approaches can improve the biocompatibility, rendering these nanomaterials suitable for biomedical applications including, but not limited to, bone-tissue engineering and regenerative medicine [139]. Ongoing research efforts are focused on reducing cytotoxicity and improving biocompatibility for the successful integration of carbon nanomaterials in future clinical applications [140]. The factors contributing to the toxicity of CNTs include oxidative stress, alterations in protein synthesis, malignant transformation, DNA damage and mutation, interstitial fibrosis, and changes in mitochondrial activity [141–143]. The interaction of carbon nanoparticles with intracellular organelles can lead to an increased production of reactive oxygen species (ROS) and trigger signaling cascades associated with inflammation [140]. Surface modification of GO with biomolecules like proteins, polymers,

and/or nucleic acids have been shown to reduce the cytotoxicity of GO [144]. Eivazzadeh-Keihan et al. [145] reviewed approaches to lowering the cytotoxicity of GO, CNT, carbon dots, nanodiamond, and fullerene to enhance the applicability of carbon nanomaterials in artificial bone tissue production and regenerative medicine. The cellular toxicological studies of carbon nanomaterials in different cell types, including macrophages, epithelial cells, and lymphocytes has been reviewed elsewhere [143,146,147].

3.3. Bioactive Glass–Ceramic Nanoparticles and Nano-Silica Hydrogels

Bioactive glass is a group of inorganic bioactive materials composed of Na_2O, CaO, P_2O_5, and SiO_2 that can improve the vascularization, osteoblast adhesion, restoration, and reconstruction of mineralized hard tissues, and differentiation of MSCs, making them suitable candidates for clinical applications [148–151]. Bioactive glass was the first biomaterial, discovered by Larry L. Hench in 1969, that could stimulate osteogenesis and bond with host tissues [152,153]. Bioactive glass–ceramics are classified as Class A bioactive materials due to their unique ability to support osteoconduction, which refers to the growth of bone along the surface of the implant. They also facilitate osteoinduction, meaning that the materials can activate and recruit osteoprogenitor cells, promoting bone growth directly on its surface [154,155]. Over the years, research has increasingly examined the potential of bioactive glass for regenerating cardiac, lung, and peripheral nerve tissues, restoring the musculoskeletal system, and promoting wound healing. Gerhardt and Boccaccini reviewed the recent developments of bioactive glass and glass–ceramic scaffolds in tissue engineering [154].

A sol–gel-derived bioactive glass nanoparticle (BGN) in a 62 SiO_2–34.5 CaO–3.2 P_2O_5 (mol %) composition was fabricated, and the structural, morphological, and elemental properties were characterized using Fourier transform infrared spectroscopy, X-ray diffraction analysis, scanning electron microscopy, elemental analysis, transmission electron microscopy, and solid-state nuclear magnetic resonance [156]. The particle size of the BGN is provided in Table 4.

Table 4. Particle size distribution of BGN synthesized using different fabrication techniques based on TEM image analysis. Reproduced from ref. [156].

	M1-P1	**M1-P2**	**M2-P1**	**M2-P2 A**	**M2-P2 B**	**M2-P2 C**
Particle size (nm)	438 ± 17	425 ± 17	86 ± 14	70 ± 13 193 ± 51 495 ± 12	18 ± 2	18 ± 5

TEM images revealed dense, monodispersed, and spherical particles of ~400 nm diameter (Table 4). M2-P2 A protocol yield an average particle size of ~70 nm (52%), ~193 nm (39%), and ~495 nm (9%), respectively, with decreasing H_2O concentration. As depicted in Table 4, stirring time changed the particle size of BGN to ~20 nm (M2-P2 B and M2-P2 C). The osteoconductive behavior of BGN was assessed via in vitro biomineralization studies. For method 1 (M1) BGNs, the vibration peaks that confirmed the presence of a calcium phosphate phase after immersion in SBF were significantly lower than the spectra of method 2 (M2) BGNs. BGNs fabricated using the M2 protocol exhibited half the network connectivity than M1 BGNs protocols due to higher calcium incorporation and underwent a faster bioactive response. The details of the fabrication process are provided in the associated reference [156].

A 3D porous bioactive glass–ceramic scaffold coated with HA-fatty acid was characterized for the first time by De Luca et al. [148] as bone tissue-engineering material. To measure the bioactivity, HA-fatty acid conjugates were deposited on the glass-derived scaffolds. The in vitro bioactivity tests showed a moderate increase in the solution pH from 7.40 to 7.56 after 1 week, which was associated with the ion release from the surface of the scaffold to the simulated body fluid (SBF). The scaffolds soaked for 48 h in SBF indicated the formation of a new phase composed of calcium phosphate globular agglomerates.

The coating of HA-fatty acid conjugate had no detrimental impact on the apatite-forming ability of the scaffolds [148]. These novel bioactive glass–ceramic scaffold biomaterials hold promise for bone repair due to their apatite-forming and tissue regenerative potential.

AuNPs/Au and Ag NPs-containing bioactive glass in alginate–pullulan composite (Alg-Pll-BGAuSP and Alg-Pll-BGAuNCs) were studied in vivo and in vitro on fibroblast and osteoblast cell lines for bone and tissue development, osteoconductivity, and bioactivity [157]. The composites exhibited a viability for the human fibroblast cell line (BJ CRL 2522TM) between 91 and 110% after 24 h. The highest viability of ~110% was obtained in presence of Alg-Pll-βTCP/HA, and Alg-Pll-BGAuSP composite (104%) had the most beneficial effects on bone proliferation [157]. Bioactive Si−Ca−P−Mo glass–ceramic nanoparticle (BBGN) with inlaid molybdate nanocrystals was synthesized for post-surgical melanoma therapy and skin reconstruction [158]. BBGN showed strong antioxidant activity, high photothermal qualities, low toxicity, and efficient infection therapy, and photothermal temperature could be achieved by changing the ratio of Mo^{4+} to Mo^{6+}. The antibacterial efficiency was studied against *Staphylococcus aureus* (*S. aureus*), *Escherichia coli* (*E. coli*), and MRSA in vitro. The three bacterial strains were not inhibited after contact with BBGN-Mo (B-M) for 12 h. The antibacterial effect for the control+ group was <10%. B-0 M with 10 min of 808 nm laser irradiation (B-0M+) demonstrated a 32.7% kill ratio for *S. aureus*, a 47.6% kill ratio for *E. coli*, and a 46.8% kill ratio for MRSA. About 98.9% of *S. aureus*, *E. coli*, and MRSA were killed after being cultured with B-15M+ groups. B-15 M glass–ceramic nanomaterials, due to their free d-electrons, presence of oxygen vacancies, and bioactive composition, demonstrated enhanced photothermal antioxidant, antibacterial, and anti-inflammatory properties, useful for post-surgical bone-infected wounds, inhibition of tumor recurrence, and tissue regeneration [158].

Khatami et al. reported the osteogenic properties of alginate-nano-silica hydrogels enriched with collagen and gelatin on human osteoblast-like MG-63 cells [159]. The osteogenic potential was measured by alkaline phosphatase activity. The addition of collagen and gelatin increased the cell proliferation rate. Biochemical analysis and Alizarin red S staining showed collagen-induced osteogenesis by induction of alkaline phosphatase and matrix mineralization. Silver-doped and gold-doped quaternary 46S6 bioactive glass (BG-Ag and BG-Au) was synthesized, and the cytotoxic effect was studied for potential bone regeneration application [160]. The BG was doped with 0.006 and 0.01 ppm concentrations of AgNPs (AuNPs) to yield BG-Ag1 (BG-Au1) and BG-Ag2 (BG-Au2) composites. Zeta potential and DLS measurements of BG and the nanocomposites showed a reduction in the hydrodynamic particle size of BG-Ag nanocomposites compared to pure BG (Table 5). BG-Ag2 had the lowest polydispersity index (PDI) of 0.262. An increase in zeta potential of the nanocomposites compared to BG was attributed to surface adhesion of Ag^{n+}. Upon incorporation of AuNPs, a decrease in particle size of BG and increase in zeta potential was attributed to the surface adhesion of Au^{n+}, which rendered the surface less negative in charge.

Table 5. Dynamic light scattering (DLS), polydispersity index (PDI), and zeta potential of bioglass and metal–bioglass nanocomposite materials. Reproduced from ref. [160].

Sample	DLS, H_D (nm) PDI		Zeta Potential (mV)
BG	626 ± 70.51	0.899	−28.9 ± 7.64
BG-Ag1	33.16 ± 3.65	0.853	−21.7 ± 7.55
BG-Ag2	85.81 ± 12.77	0.262	−24.5 ± 4.69
BG-Au1	59.19 ± 10.03	0.789	−12.6 ± 4.85
BG-Au2	92.54 ± 13.80	0.789	−16.5 ± 5.81

The proliferation of osteosarcoma MG-63 cells with different concentrations of BG, BG-Ag1, BG-Ag2, BG-Au1, and BG-Au2 at 0, 2, 4, 6, 8, and 10 µg/mL dosage was considered. Cell proliferation increased even at low concentrations compared to the control group. At a dosage of 6 µg ml^{-1}, the cell proliferation was 141.25%. With increase in dosage to 8 and

10 μg ml^{-1}, the proliferation declined to 128.40% and 128.61%, respectively. This affirmed the biocompatibility of BG and metal-doped BG nanohybrids with MG63 cells [160].

Hydrogels based on mesoporous silica nanoparticles (MSNs), due to their porous homogeneous structure, biocompatibility, high surface area, and tunable core and shell chemistry, serve as ideal candidates in regenerative medicine, as they can mimic the ECM of native tissues [161]. A MSN-PEG nanocomposite hydrogel formed by dynamic covalent crosslinking of thiol surface-functionalized MSNs with thiol-modified polyethylene glycol was developed [161]. The mechanical and self-healing properties of these 3D networks were investigated via macroscopic self-healing and rheological recovery tests. A 7 wt. % of MSN concentration did not influence the self-healing behavior, and recovery of MSN7-PEG hydrogel decreased after applying 500% strain, primarily due to the higher MSN content. The degradation behavior of the hydrogels was measured in PBS buffer or GSH (glutathione). In the presence of GSH, which is a reducing agent, the disulfide bonds in the nanocomposite hydrogels were prone to degradation. MSN2-PEG showed ~80% loss of mass in presence of 300 μM GSH but no significant mass loss in PBS. However, MSN-PEG hydrogels exhibited slow degradation in 300 μM GSH in MSN-PEG nanocomposites, which was due to increased crosslinking density of the MSNs within the polymeric network.

3.4. Calcium Phosphates

Calcium phosphate (CaP)-based biomaterials are widely researched for cell attachment, proliferation, and differentiation in bone defect repair due to their resemblance to the chemical composition of natural minerals [162]. Various CaP-based biomaterials have been utilized in bone regeneration, including tricalcium phosphate, HAP, amorphous calcium phosphate, octacalcium phosphate, dicalcium phosphate anhydrous, dibasic calcium phosphate dihydrate, and tetracalcium phosphate [163]. HAP is the most thermally stable crystalline phase of CaP used in the form of ceramics or composite scaffolds with polymers [162]. Zhi et al. [164] synthesized a biomimetic and injectable hydrogel scaffold based on nano-HAP, collagen (Col), and chitosan (Chi) as workable systemic minimally invasive scaffolds in bone defect repair and bone tissue engineering. The results from SEM, TEM, and XPS suggested that Chi/HA/Col exhibited surface properties akin to physiological bone, and the peaks in the FT-IR spectrum corresponded to those found in natural bone. A mixture of palladium (Pd) and platinum (Pt) nanoparticles, called PAPLAL, was studied for aging-related skin pathologies in mice [165]. PAPLAL did not cause any morphological abnormalities, such as cell infiltration, deposition or cellular damage in mouse skin and exhibited potent antioxidant activity (attributed to the effects of Pt nanoparticles) and attenuated aging-related skin pathologies in vivo.

Non-woven multifunctional nano- and microfiber scaffolds were fabricated using a block copolymer of PCL and poly(lactic acid) (PLA) (PL-b-CL) as a matrix and HAP as a functional agent, dissolved in a binary solvent mixture to produce electrospun scaffolds with porous fibers [166]. The nanofibrous scaffolds were shown to mimic the ECM of bone. As an in vitro model of mature osteoblasts, SaOS-2, an osteosarcoma cell line, displayed osteoblastic capacity to deposit a mineralization-competent ECM. The cells grown on scaffolds with HAP exhibited higher metabolic activity than pristine PL-b-CL. Cell adhesion results suggested that the cells adhered and proliferated, with no substantial cell loss during the experimental period. Cell attachment was influenced by the physical and chemical properties of the scaffolds, namely, functional groups, solubility, crystallinity, electric charge, surface energy, surface roughness, topography, pore size, and stiffness. This was the first study to demonstrate that scaffolds created from a PCL and PLA block copolymer with embedded HAP NPs could enhance the potential of scaffolds for bone tissue engineering applications [166].

Chitosan (CS) hydrogel reinforced with hydroxyapatite nanorod (HAPNr) composite materials was developed for biomedical hydrogels and articular cartilage regeneration [167]. HAPNr incorporated into the CS matrix demonstrated improved mechanical properties, with the best results obtained for CS/1.5HAPNr composites. The cytotoxicity of the

composite hydrogel towards L929 cell lines was measured in vitro. Phytohaemagglutinin (PHA)-treated composite had the highest cell viability of 112% and CS/1.5 HAPNr showed better cell proliferation (96 ± 0.41%) than pristine CS hydrogel (90 ± 0.63%) due to the release of Ca^{2+} and PO_4^{3-} ions from HAP that helped anchor CS hydrogel. L929 mouse fibroblast cells exhibited a fusiform morphology, and most cells spread and proliferated on the culture plate. The hydrogels exhibited no apparent cytotoxicity towards L929 cell lines, and the cells proliferated uniformly on the culture plate and exhibited a fusiform morphology. The CS/1.5HAPNr composite hydrogel may serve as a potential biomaterial for tissue engineering cartilage regeneration.

A biphasic cartilage and bone-like scaffold combined with HAP was developed for osteochondral tissue engineering [168]. Three types of self-assembled biphasic artificial cartilage–HAP conjugates from cartilage components, hyaluronic acid (HA), aggrecan (AG), and type II collagen were implanted in vitro into an osteochondral defect in rat knee joints, bone, and cartilage tissues (Figure 6A). The SEM micrographs revealed a fibrous 3D reticulate structure (Figure 6B). Incubation of the chondrocytes with AG/HA/collagen complex for 1 or 2 weeks showed the chondrocytes to be uniformly distributed on the scaffold. On the surface of the self-organized scaffolds, cytoplasmatic extensions denominated the phylopodia, hinting that the chondrocytes were alive after the 2-week incubation (Figure 6C).

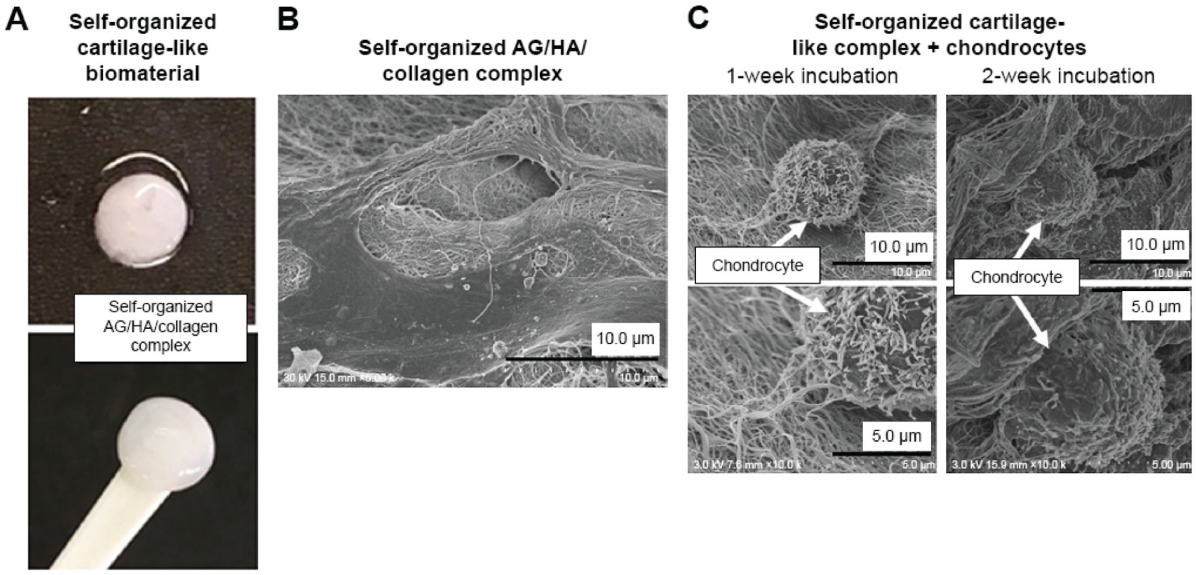


Figure 6. Self-organized cartilage-like scaffold formed from HA, AG, and type II collagen for articular cartilage tissue engineering. (**A**) Macroscopic image of self-organized cartilage-like scaffold. (**B**) Self-organized AG/HA/collagen complex as observed by SEM. (**C**) After 1- and 2-week incubation of chondrocytes with the self-organized AG/HA/collagen complex, chondrocytes were present on the scaffold of fibers forming the complex. Reprinted with permission from ref. [168]. This work is published and licensed by Dove Medical Press Limited. The full terms of this license are available at https://www.dovepress.com/terms.php and incorporate the Creative Commons Attribution–Non-Commercial (unported, v3.0) License (http://creativecommons.org/licenses/by-nc/3.0/, accessed on 1 November 2024).

To investigate the role of scaffold implantation in knee cartilage defects, in the control right knee joints, cartilage defects were filled with scar tissue and clefts were present between the scar and healthy surrounding tissue. In the left knee joints, cartilage defects were filled with repair tissue similar to the surrounding cartilage tissue. In knee joints without implant (sham-operated), fibrous scar tissue with hyperplasia of spindle-shaped fibroblastic cells was observed with no regeneration of cartilage tissue in 4 or 8 weeks. In left knee joints with implanted scaffolds, a stratiform cartilage-like structure with the

formation of cartilage cavities and the growth of chondrocytes was observed in the implantation hole, pointing to cartilage regeneration. The osteochondral tissue regeneration rate was 33% in the AG/HA/collagen group, 50% in AG/HA/collagen complex–HAP powder (40 nm size), 75% in AG/HA/collagen complex–HAP powder (5 μm size), and 100% in the AG/HA/collagen complex–HAP block conjugate-implanted group [168]. Cartilage-like scaffold without conjugated HAP was insufficient to regenerate damaged subchondral bone tissue. The self-organized cartilage-like biomaterial conjugated with HAP not only repaired articular cartilage defects but also the degenerated subchondral bone in osteochondral defects.

Nanocrystalline hydroxyapatite (nHAP) was utilized to demonstrate how the differentiation of hMSCs was affected by nHAP loading and induced by bone-like scaffolds [169]. The nHAP dispersed in polymeric composites at >22 wt. % loading induced osteoblast differentiation in vitro via the PiT1 and Erk1/2 signaling pathways. When nHAP-poly(thioketal urethane) nHAP-PTKUR scaffolds were implanted in two anatomic sites in rats, namely, the femoral diaphysis and femoral metaphysis, new cartilage was formed in the absence of nHAP at the diaphyseal but not at the metaphyseal sites. New bone formation increased with nHAP loading at metaphyseal but not diaphyseal sites. Thus, nHAP composite scaffolds induced osteogenic differentiation of adherent endogenous progenitor cells in a dose-dependent manner. nHAP-PTKUR scaffolds promoted intramembranous and endochondral ossification dependence on material formulation and anatomic sites, indicating the importance of these factors as key regulators in assessing overall outcomes and the efficacy of novel biomaterials for bone regeneration.

Huang et al. [170] developed a gelatin/HAP-based hydrogel material using microextrusion 3D bioprinting and enzymatic cross-linking to promote the proliferation of human umbilical cord blood-derived mesenchymal stem cells (hUCB-MSCs) and repair of knee cartilage defects. To produce bioink for 3D-printed gelatin scaffolds, 10% of gelatin with 5% volume weight of HAP provided the best gelation kinetics and rheological properties. Two types of scaffolds, namely, 10% of gelatin and 10% of gelatin with 5% volume weight of HAP, was used in the study. SEM images showed porosity rates of 85.26 $\pm$ 2.09% for the gelatin scaffold and 81.29 $\pm$ 2.05% for the gelatin/HAP scaffold. The cytotoxicity was measured by culturing hUCB-MSCs in the extracted solutions of the scaffolds (Figure 7A). The extract solutions supported a high cell viability of >75%, as shown in Figure 7B. A continuous increase in cell population confirmed that the extracted solutions of scaffold-facilitated cell proliferation and migration of hUCB-MSCs (Figure 7C). The 3D printing of gelatin scaffolds assisted by enzymatic cross-linking and HAP doping strengthened the ability of the gelatin scaffold to enhance chondrogenic differentiation of stem cells and regeneration of bone and cartilage.

Biocompatible nanocomposite materials based on chitosan, HAP, and riboflavin have shown high antioxidant activity and inhibitory effect on *Staphylococcus aureus* compared to pure chitosan, useful in cell adhesion and the tissue regeneration process [171]. Riboflavin (RF) increased the antioxidant activity of Cs/HAP/RF composite material compared to pure Cs and HAP–doped Cs and reduced the inhibitory effect on *Staphylococcus aureus*. MTT assay provided insights into the effect of different concentrations of RF on cell metabolic activity of mouse embryonic fibroblasts (NIH3T3) and human osteosarcoma (U-2OS) cell lines. Cell migration/mobility response of NIH3T3 cell lines were accessed at different concentrations of riboflavin for 48 h of exposure. The scratch closure of NIH3T3 cells was close to 100%, suggesting riboflavin to have no negative effect on cell migration; rather, it activated cell proliferation process [171].

Chitosan–collagen–HAP (Cs/Col/HAP) composites are bioactive, biocompatible, and multifunctional biomaterials that find application in tissue engineering [172]. SEM micrographs of the composite membrane showed the Cs membrane to align as fibers with pore sizes of 80 nm to 2 μm. Incorporation of collagen changed the morphology of the Cs membrane; at low collagen content, pleats were formed, and areas surrounded by fibers suggested that collagen regions were blended into the chitosan matrix. At high collagen

content, a uniform morphology was observed, characteristic of polymer blends. The cell viability was measured by MTS for buccal fat pad (hBFP)-MSCs. The membranes with the highest collagen and/or HAP content showed the highest cell adhesion values for in vitro-cultured hBFP-MSC. The membranes with low collagen and/or low HAP content showed similar cell viability compared to pure chitosan membranes. The largest cell viability was obtained when both compounds were present in the chitosan membrane with the highest collagen and HAP (Cs/0.75 collagen/0.75 HAP) content, showing 75% higher viability than pure chitosan. This study proposed that membranes obtained by combining chitosan with collagen and HAP enhanced cell adhesion ability, compared to the chitosan membranes alone.

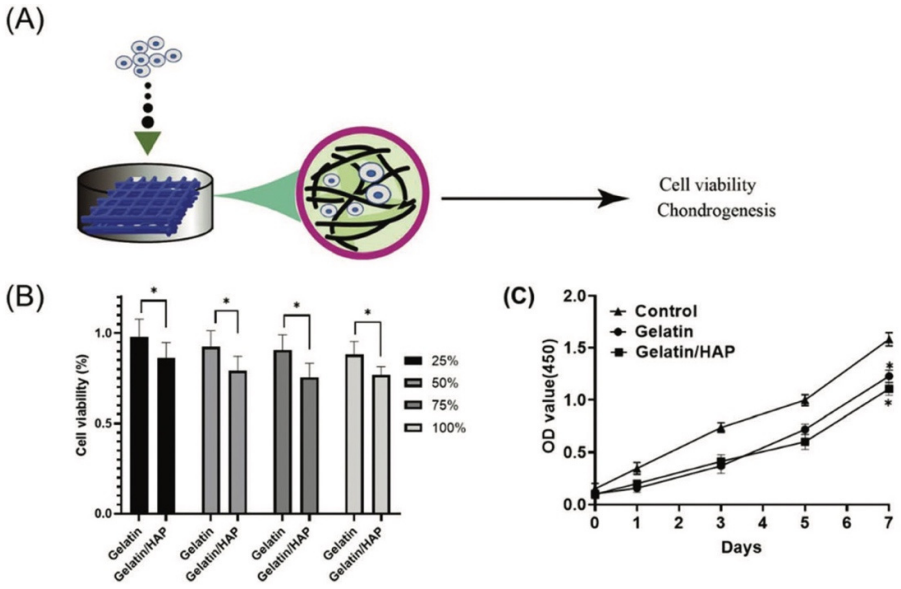


Figure 7. Proliferation and induction of hUCB-MSCs on scaffolds. (**A**) Schematic illustration of the experimental design of differentiation of human umbilical cord blood-derived mesenchymal stem cells (hUCB-MSCs). (**B**) Cytotoxicity measurement of the scaffold extraction solutions. *, $p < 0.05$. (**C**) The proliferation of hUCB-MSCs cells on the scaffold material shows a continuous increase in cell population. Reprinted with permission from ref. [170] from Royal Society of Chemistry.

A partially crystallized CaP and dicalcium phosphate anhydrate particle, integrated with black phosphorous nanosheets, was used to prepare calcium phosphate bone cements (CPCs) for potential application for bone regeneration [173]. The physicochemical, photothermal, biodegradability, cytotoxicity, and osteoinductive properties of CPCs were investigated to develop an innovative bone defect repair material. SEM images were analyzed to observe the adhesion of MC3T3-E1 cells on the surface of bone cement (BP/CPC) after co-culture for 1 and 24 h. At 1 h, cell morphology on the CPC surface was spherical, but on the 100 BP/CPC surface, the morphology was irregular. On the 200 BP/CPC surface, the morphology of cells was similar to that of 100 BP/CPC, and there were more pseudopodia. After 24 h of coculture, cells on the three bone cements were long and spindle-shaped, with the appearance of plate pseudopodia and filamentous pseudopodia. The BP/CPC successfully promoted cell adhesion in the early stages and demonstrated its biocompatibility. The addition of black phosphorus enhanced the strength of the bone cement. BP/CPC induced cell growth and showed very low to no toxicity for MC3T3-E1 cells. Experiments on osteoblast development showed that BP/CPC under near-infrared conditions accelerated the mineralization of bone cement and promoted the upregulation of osteogenic marker proteins in cells.

3.5. Magnesium Oxide Alloys

Magnesium (Mg) alloys can stimulate bone formation, increase new bone quality, promote the growth of bone tissues, and induce bone cell activation [174–176]. Degradable Mg alloys are of particular interest, as Mg can degrade under physiological conditions and eliminate the requirement for secondary surgical removal [127,177]. Mg-based implants are also efficient in stabilizing fractures and aiding healing process [178]. Liu et al. [175] studied the osteogenesis, angiogenesis, and antibacterial properties of Mg-Cu alloys, namely, Mg-0.05Cu, Mg-0.2Cu, and Mg-0.5Cu for orthopedic applications. Cell viability of pre-osteoblasts (MC3T3-E1) and endothelial cells (HUVECs) towards Mg-Cu alloys and pure Mg extraction media was studied for 24 h of incubation. Pre-osteoblast viability of Mg-0.03Cu and Mg-0.19Cu alloys were >100%, whereas Mg-0.57Cu had a slightly smaller value than pure Mg and other alloys. Increasing Cu concentrations in the Mg-Cu alloy decreased HUVECs viability from 125 to 75%. The results suggested that Mg-0.03Cu and Mg-0.19Cu stimulate the growth of MC3T3-E1 and HUVECs cells. Cell proliferation of MC3T3-E1 and HUVECs in the extraction media of Mg-Cu alloys and pure Mg was studied. On day 1, the control groups, pure Mg and its alloys did not show any difference in cell number in MC3T3-E1 cells. Mg-Cu alloys indicated less cell proliferation after 3 and 5 days. Cu depressed MC3T3-E1 cell proliferation. In HUVECs, Mg-0.03Cu showed the most cell proliferation after 1, 3, and 5 days, while Mg-0.57Cu exhibited the opposite response. Cell adhesion studies on cytoskeletons of MC3T3-E1 cells after 12 h of immersion in the extracts revealed spreading and superior filopodia extension for pure Mg and Mg-Cu alloys when compared to control. Compared to pure Mg and Mg-0.57Cu, MC3T3-E1 cells cultured in Mg-0.03Cu and Mg-0.19Cu extracts had more plump focal adhesion via well-organized F-actin stress fibers. The aggregation of HUVECs diminished with increasing Cu concentration, and cell status deteriorated slightly. This indicated that Mg-0.03Cu and Mg-0.19Cu extracts are favorable for initial attachment and spreading of HUVECs and MC3T3-E1 cells. The combined effects of high alkalinity and copper release from biodegradable Mg-Cu alloys, along with their enhanced mechanical and antibacterial properties compared to pure Mg, make these alloys suitable for stimulating osteogenesis and angiogenesis in orthopedic applications.

Saha et al. [127] reported the conformal deposition of MgO films on collagen using ALD technique at room temperature. This was done to improve the osteointegration and reinforce the mechanical strength and biocompatibility of collagen. Biocompatibility analysis of the membranes did not reveal any foreign body reactions in Col (control), Col-MgO200, and Col-MgO500 experimental samples. The Col-MgO200 and Col-MgO500 groups showed higher lymphocyte count compared to Col ($p < 0.05$), and coated groups showed similar results (Col-MgO200 = Col-MgO500; $p > 0.05$). Data from inflammatory profiles and blood cell counts suggested the following order: Col-MgO500 > Col-MgO200 > Blood clot—BC (negative control) > Col groups. BC had the lowest number of lymphocytes, while Col-MgO200 had the highest number (Col-MgO200 > Col-MgO500 = Col > BC) at 14 days, and higher inflammatory cells were found for Col-MgO200 group at 28 days as well. Histology characteristics of bone healing at 7-, 14-, and 28-day periods indicated that BC forms few newly formed bones until 28 days. Col-MgO200 and Col-MgO500 groups facilitated osteopromotive properties with increased osteoblastic activity, and Col-Mg200 and 500 showed good compatibility in the subcutaneous tissues. This study hinted at the need for pre-clinical assessments to confirm membrane compatibility and bone reconstruction.

Li et al. [176] reported the post-degradation effect of pure Mg, Mg-1Y, Mg-5Al, and Mg-2Ca alloys for the differentiation, proliferation, and gene expression of human mesenchymal stem cells (hMSCs). Mg^{2+} ions increased cell proliferation, and a maximum concentration of approximately 8.0×10^{-4} M was favorable for ATP production, above which ATP production decreased. Mg-2Ca alloy had minimal effect on osteogenic differentiation, with Mg-1Y and pure Mg having a superior effect on the proliferation and differentiation of hMSCs.

An immunomodulatory multicellular scaffold based on manganese silicate (MnS) nanoparticles with tendon/bone-related cells was fabricated for integrated regenerative recovery of tendon-to-bone injury [179]. The MnS nanoparticles were shown to enhance the specific differentiation of multicellular scaffolds via regulating macrophages. This was attributed to the secretion of PGE2 in macrophages induced by Mn ions. The tendon stem/progenitor cells (TSPCs) and BMSCs were distributed in a layered manner and the multicellular MnS-based nanoparticle scaffolds were implanted into macrophage-depleted rats to reveal the role of immunomodulatory processes in the differentiation of scaffolds. The Mn ions stimulated macrophages to secrete more PGE2, and a notable enhancement in the secretion of PGE2 in macrophages suggested that Mn ions could induce the secretion of PGE2 in macrophages to enhance the tenogenic differentiation of TSPCs and osteogenic differentiation of BMSCs.

3.6. Gold Nanoparticles

Gold nanoparticles (AuNPs) proffer tunable size, surface functionalization, unique physiochemical properties, and surface plasmon resonance with light at a wavelength of 520 nm [180], making it a suitable entrant in biomedicine, drug delivery, and imaging [181,182]. Using coarse-grained molecular dynamics, Gupta and Rai [183] provided molecular level insights on the permeation free energy of dodecanethiol-coated neutral hydrophobic AuNPs of 2–5 nm dimension via a model skin lipid membrane (Figure 8). Charged AuNPs were adsorbed on the bilayer headgroup, while neutral hydrophobic AuNPs disrupted the bilayer and penetrated inside. AuNPs of 2 nm did not cause any structural changes in the bilayer. However, larger AuNPs, ranging from 3 to 5 nm, significantly altered the structure and packing of the bilayer. Some lipids from the bottom leaflet formed a hump-like structure to accommodate these bigger nanoparticles. The permeability was maximum for neutral 2 nm AuNP and minimum for 3 nm cationic AuNP. AuNPs created vacancies in the bilayer interior and induced undulation that increased with nanoparticle size. The permeation-free energy calculation suggested a very small barrier for neutral hydrophobic AuNP at the head group of the bilayer, while a free energy minimum was observed for charged AuNPs. Neutral hydrophobic AuNPs created more disruptions in the bilayer, which reduced the local and overall order parameter of the bilayers. The smaller neutral hydrophobic AuNP was more permeable, and charged AuNPs experienced resistance to permeation in the bilayer interior.

Lin et al. [181] investigated the biocompatibility and cell viability of AuNPs towards MSCs by analyzing the optimal AuNP concentration for tissue engineering efficacy. The % cell viability of MSCs at different AuNP concentrations of 1.25, 2.5, 5, and 10 ppm were investigated at 24, 48, and 72 h, respectively (Figure 9A). AuNPs at 1.25 and 2.5 ppm stimulated the lowest intracellular ROS generation, while AuNP at 10 ppm induced the highest production of ROS at time points of 24 and 48 h (Figure 9B,C). Fluorescence images of MSC cell adhesion stimulated by the AuNP solutions showed MSCs' morphology to be filopodia and lamellipodia in both the 1.25 and 2.5 ppm AuNPs, demonstrating improved cell adhesion and migration capacity. AuNPs at concentrations of 1.25 and 2.5 ppm demonstrated better biocompatibility. The AuNPs fabricated with polymeric biomaterials exhibited superior biosafety and reduced toxicity beneficial in clinical applications.

AuNPs enhanced the differentiation of osteoblastic MC3T3-E1 cells and antimycin A-induced mitochondrial dysfunction, as demonstrated by an MTT assay [184]. The MC3T3-E1 pre-osteoblastic cell line is widely used as a cell culture model for osteoblast differentiation. A significant increase in cell growth was revealed by the treatment of 5, 10, and 20 nm AuNPs at the concentrations of 1~10, 2~10, and 1~10 μg/mL, respectively, which suggested that AuNPs did not induce any cytotoxicity and stimulated osteoblast growth. AuNPs with a diameter of 10 nm considerably promoted osteogenesis through activating earlier osteogenic differentiation. Thus, AuNP increased the bone matrix by stimulating ALP activity, collagen synthesis, and osteocalcin synthesis in osteoblastic MC3T3-E1 cells. AuNPs (a) had a protective effect against oxidative stress-induced dysfunction in

osteoblasts, (b) had a stimulating effect on the early differentiation stages of osteoblasts, and (c) protected osteoblasts from antimycin A-induced cell damage.

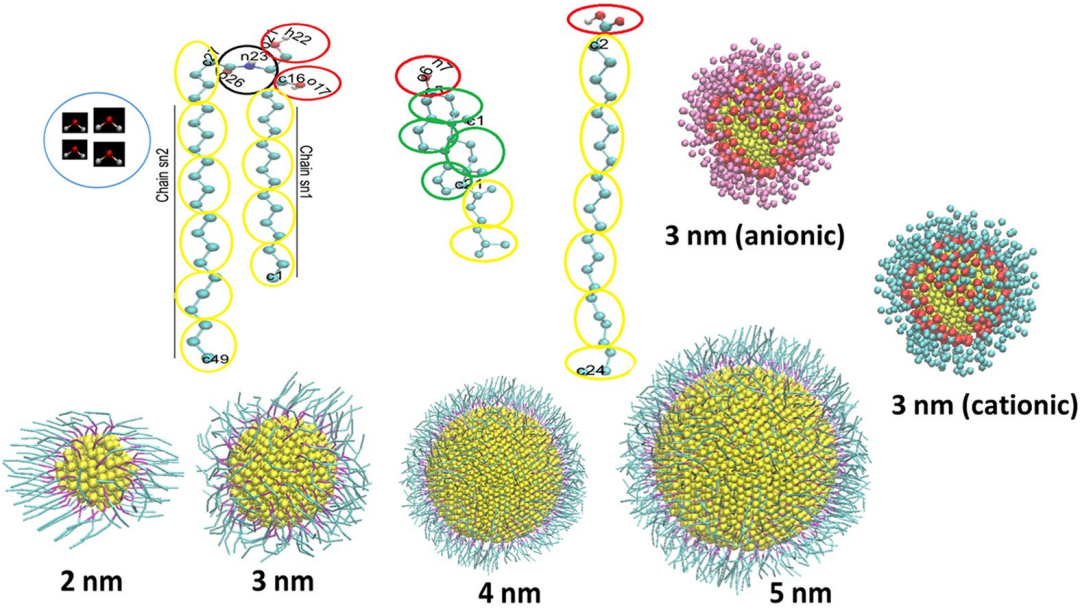


Figure 8. Coarse-grained molecular structures of long-chain ceramides, cholesterol, and fatty acids of skin lipid matrix, water, and thiol-coated AuNPs used in the simulations. Reproduced from ref. [183]. This work is licensed under a Creative Commons Attribution 4.0 International License, http://creativecommons.org/licenses/by/4.0/ (accessed on 1 November 2024).

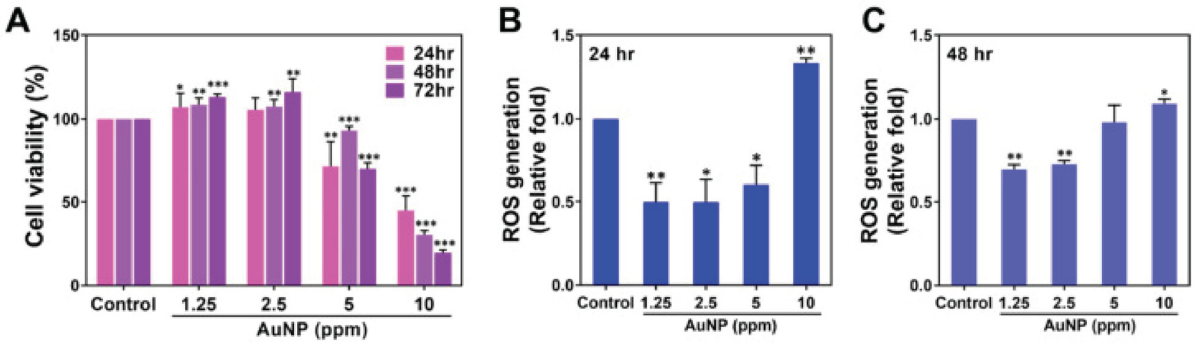


Figure 9. The cell viability and ROS generation of MSCs with different concentrations of AuNPs. (**A**) The cell viability of MSCs treated with AuNPs indicated that AuNP 1.25 and 2.5 ppm treatments enhanced MSC proliferation at 48 and 72 h, while the AuNP 5 and 10 ppm treatments had significantly lower cell viability. (**B**,**C**) Intracellular ROS generation in MSCs was detected using the FACS method after 24 and 48 h of treatment. AuNP 1.25 and 2.5 ppm induced lower ROS production at both time points. The results are displayed as mean ± SD (n = 3). * $p < 0.05$, ** $p < 0.01$, *** $p < 0.001$: compared to the control group (TCPS). Reproduced from ref. [181]. Licensee MDPI, Basel, Switzerland. This article is an open access article distributed under the terms and conditions of the Creative Commons Attribution (CC BY) license, https://creativecommons.org/licenses/by/4.0/ (accessed on 1 November 2024).

In soft tissue augmentation, AuNP-collagen constructs (AuNP-CC) were applied as soft tissue fillers to investigate the biodegradability and local tissue reaction of AuNP-collagen fillers compared to commercially available HA and cross-linked collagen fillers [185]. Two conjugates were constructed: AuNP-CC1, fabricated with the addition of 10% of pre-polymerized porcine Type I collagen; and AuNP-CC2, fabricated with the addition of 3% glycerin. The tissue response (neovascularization and granulation tissue) scores for the cohorts were investigated at 1, 3, and 6 months. Cross-linked collagen, AuNP-CC1,

and AuNP-CC2 demonstrated slight to mild neovascularization and scored in the mild to moderate range for granulation tissue. The AuNP-CC formulations scored in the slight to mild range for granulation tissue. By 6 months, the cross-linked collagen demonstrated mild to moderate neovascularization and was in the mild range for granulation tissue. The AuNP-CC formulations scored slight to mild in each category. Cross-linked collagen showed increased tissue response scores over time. AuNP-CC2 had a similar response with increasing tissue response scores; however, the irritancy scores were more stable over time. These responses indicated active resorption of the constructs along with active remodeling [185].

The biomedical applications of AuNPs have been extended to wound-healing process [186,187]. Poomrattanangoon and Pissuwan [188] synthesized AuNPs coated with Collagen-I (Collagen-I@AuNPs) and studied the efficacy towards human skin fibroblast (HSF) cells for wound closure, cell proliferation, pro-inflammatory responses, growth factor generation, and in vitro wound healing. AuNPs and Collagen-I@AuNPs at 3, 5, 10, 15, and 25 μg mL^{-1} concentrations were applied to HSF cells, and cell viability was measured for 24 h. Attenuated total reflectance (ATR)-FTIR measurements confirmed a change in the structure of Collagen-I and AuNPs resulting from the interaction between Collagen-I and AuNPs. For HSF cells treated with Collagen-I@AuNPs, cell viability was slightly higher than cells treated with AuNPs (Figure 10). The % cell viabilities of HSF cells after treating with 3, 5, 10, 15, and 25 μg mL^{-1} of Collagen-I@AuNPs were 100.38 ± 3.51, 101.87 ± 2.40, 101.43 ± 2.32, 97.18 ± 2.25, and 97.40 ± 1.18%, respectively (Figure 10b). HSF cells treated with AuNPs at concentrations of 15 and 25 μg mL^{-1} showed a significant reduction in cell viability (95.08 ± 0.68 and 96.18 ± 0.56%) compared to control that suggested that AuNPs and Collagen-I@AuNPs are non-cytotoxic.

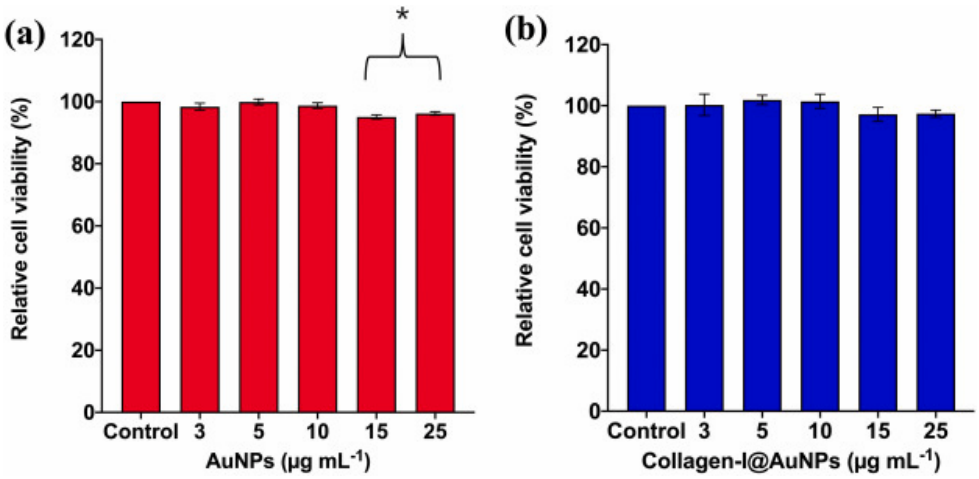


Figure 10. Relative cell viability of HSF cells treated with (**a**) AuNPs and (**b**) Collagen-I@AuNPs. The asterisk indicates a significant difference in cell viability compared to untreated HSF cells (control; $p < 0.05$). Statistical analysis was performed using Tukey_Kramer ($n \geq 7$). Reprinted with permission from ref. [188] from Elsevier. This article is under a Creative Commons license, http://creativecommons.org/licenses/by-nc-nd/4.0/ (accessed on 1 November 2024).

To study the effects of AuNPs and Collagen-I@AuNPs on wound closure, in vitro measurements using a wound scratch assay were performed [188]. The % wound closures of scratched HSF cells treated with 3 μg mL^{-1} AuNPs and Collagen-I@AuNPs for 24, 48, and 72 h are shown in Figure 11a, and images of cell migration are shown in Figure 11b. The scratched HSF cells treated with 3 μg mL^{-1} AuNPs and Collagen-I@AuNPs had a higher wound closure percentage than untreated control cells. After 24 h treatment of scratched HSF cells treated with AuNPs and Collagen-I@AuNPs, the percentages of wound closure were ~57.16 ± 1.31 and ~67.67 ± 1.67%, respectively (Figure 11a). Collagen-I@AuNPs accelerated the healing process of scratched HSF cells compared to AuNPs. After 48 h, the

percentage of wound closure in scratched HSF cells treated with AuNPs (91.01 ± 2.71%) and Collagen-I@AuNPs (95.19 ± 1.67%) increased compared to 24 h (Figure 11a). The percentage of wound closure in untreated cells increased to 59.96 ± 2.66%. Complete closure in scratched HSF cells treated with AuNPs or Collagen-I@AuNPs was observed for 72 h of treatment. This implied that Collagen-I protein was vital in enhancing wound closure, and enhanced wound closure of scratched HSF cells treated with AuNPs may be attributed to the antioxidative properties of AuNPs vital in cell migration and healing [188].

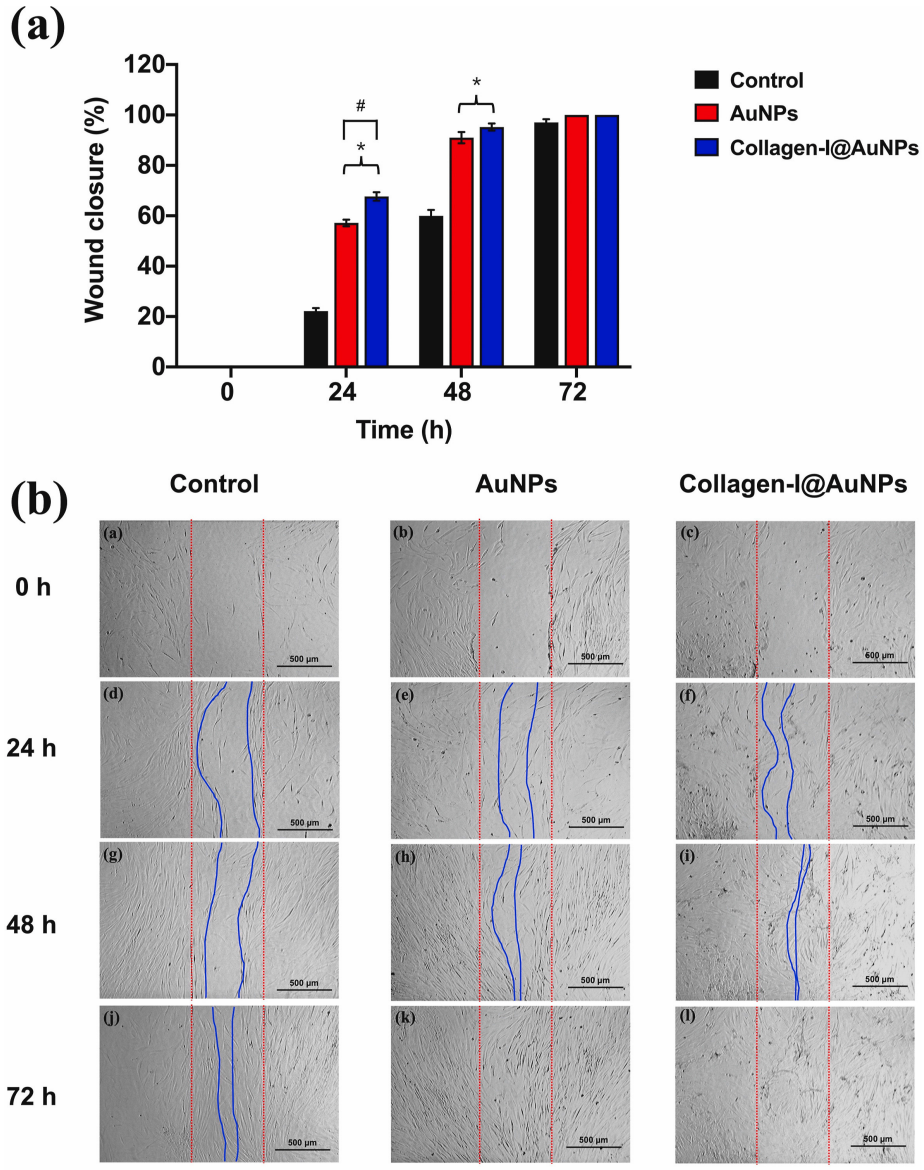


Figure 11. (**a**) Percentage of wound closure of scratched HSF cells treated with 3 µg mL^{-1} AuNPs and Collagen-I@AuNPs for 24, 48, and 72 h. * Significant difference in wound closure percentage at $p < 0.05$ compared with control cells (untreated HSF cells) at 24 and 48 h, respectively. # Significant difference in wound closure percentage of HSF cells treated with AuNPs and Collagen-I@AuNPs for 24 h, at $p < 0.05$. Statistical analysis was performed using the Tukey–Kramer test ($n \geq 11$). (**b**) Cell migration images of scratched HSF cells treated with 3 µg mL^{-1}AuNPs and Collagen-I@AuNPs for 24 h, 48 h, and 72 h. The panels (**a**–**l**) denote the cell migration images of control, AuNPs, and Collagen-I@AuNPs at 0, 24, 48, and 72 h, respectively. The figure and caption are reprinted with permission from ref. [188] from Elsevier. This article is under a Creative Commons license, http://creativecommons.org/licenses/by-nc-nd/4.0/ (accessed on 1 November 2024).

While the therapeutic and biomedical applications of AuNPs are well established, research has shown that the cytotoxicity of AuNPs is influenced by composition, size, shape, surface charge, and cell type [189]. The size of AuNPs was shown to impact ubiquitin proteasome system (UPS) such as the ubiquitin-specific protease (USP) and ubiquitin carboxyl-terminal hydrolase L1 (UCHL-1) and impact the proliferation of A549 cells [189]. A study on the size-dependent cytotoxicity of polyethyleneglycol (PEG)-coated gold nanoparticles (AuNPs) in mice found that particles sized between 10 and 60 nm had harmful effects, such as changes in cell shape, inhibition of cell proliferation, and DNA mutations [190]. In contrast, particles sized between 5 and 30 nm showed no signs of toxicity. Negatively charged (citrate-capped) and positively charged (cysteamine-capped) gold nanoparticles (AuNPs) induced cell death in a dose-dependent manner [191]. The negatively charged AuNPs caused a gradual process of cell death, while the positively charged AuNPs led to abrupt destruction of MDA-MB-231 cells. This rapid cell death was associated with increased phosphorylation of histone H3 at serine 10, indicating mitotic catastrophe [191]. Anti-proliferative activity and cytotoxicity of AuNPs on MCF7 human breast cancer cells was reported by Paramasivam et al. [192].

3.7. Biomimetic Natural Biomaterials

Biomimetic biomaterials are classified as scaffolding materials that provide the structural basis for cells to adhere, migrate, and proliferate [193]. They mimic the characteristics of the natural ECM and are currently used in various applications, including implantable materials, drug delivery systems, orthopedics, and musculoskeletal tissue engineering [193–195]. Liu et al. reviewed recent advances in the fabrication, functionality, and potential applications of biomimetic natural biomaterials [196]. Ma reviewed the importance and broad implications of current biomimetic materials and novel processing technologies in tissue engineering and regeneration [197]. Biomimetic natural biomaterials are combined with tissue engineering applications due to their non-toxicity, non-genotoxicity, and non-teratogenicity effects to healthy native tissue. Polylactic acid, polyhydroxyalkanoates and their derivatives, HA, alginate, cellulose, and chitosan, as well as collagen, gelatin, fibroin, poly-glutamic acids, and antimicrobial peptides, are the commonly used biomimetic natural biomaterials [194]. The development of biomimetic natural biomaterials that replicate the biological and physicochemical characteristics of the natural ECM integrates additional functionality and therapeutic effects, as illustrated in Figure 12.

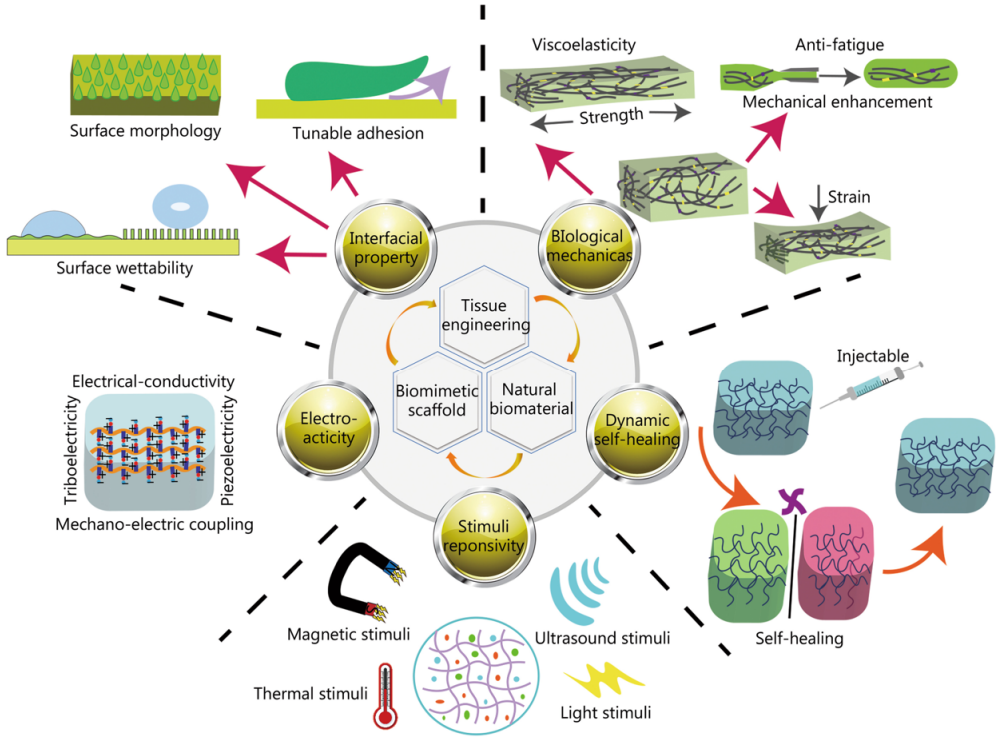


Figure 12. The innovative strategies involved in the rational design of biomimetic natural biomaterials that can mimic the ECM of tissues. Reproduced from ref. [196]. This article is licensed under a Creative Commons Attribution 4.0 International License, http://creativecommons.org/licenses/by/4.0/ (accessed on 1 November 2024).

4. Challenges in the Use of Inorganic Biomaterials in Regenerative Medicine

Clinical application of inorganic biomaterials in regenerative medicine confronts challenges, including, but not limited to, long-term fate in biocompatibility and bioaccumulation, nanoparticle/nanomaterial toxicity, better assessment tools, optimization of the mechanical properties, stem cell fate, and so on. The toxicity, carcinogenicity, bioaccumulation, and teratogenicity of nanoparticles are dose- and exposure-dependent [75]. Advances in materials science and engineering technology for the design and application of biomimetic 3D-printed degradable scaffolds have paved the way for pioneering research strategies in regenerative therapy [198]. For example, a biocompatible, high-performance semicrystalline polymer, poly (ether-ether-ketone) (PEEK), named bone cement, was one of the most prominent candidates in bone implants approved by the FDA [199,200]. Since PEEK is chemically inert and has poor integration, incorporating bioactive metals such as strontium or hydroxyapatite could stimulate cell differentiation [200,201]. Thus, the design and development of 'immune interactive' biomaterials can minimize immune response [202], such as mediating macrophage polarization, decreasing body rejection, and governing the outcome of tissue engineering and regenerative therapy [200].

Lele et al. [203] performed a detailed study of engineered biomaterials for different clinical trials and specific diseases. Ophthalmic disease had the highest number of clinical trials, followed by diseases of blood vessels and the oral cavity (Figure 13). Clinical trials suggested that synthetic polymers can be used in the fabrication of contact lenses in the treatment of ophthalmic diseases, while natural polymers can be used in the treatment of skin diseases. Dental applications utilized autologous biomaterials, ceramics, and composites. Metals and combination materials, such as polymers coated on metals, are ubiquitous for treating coronary artery disease.

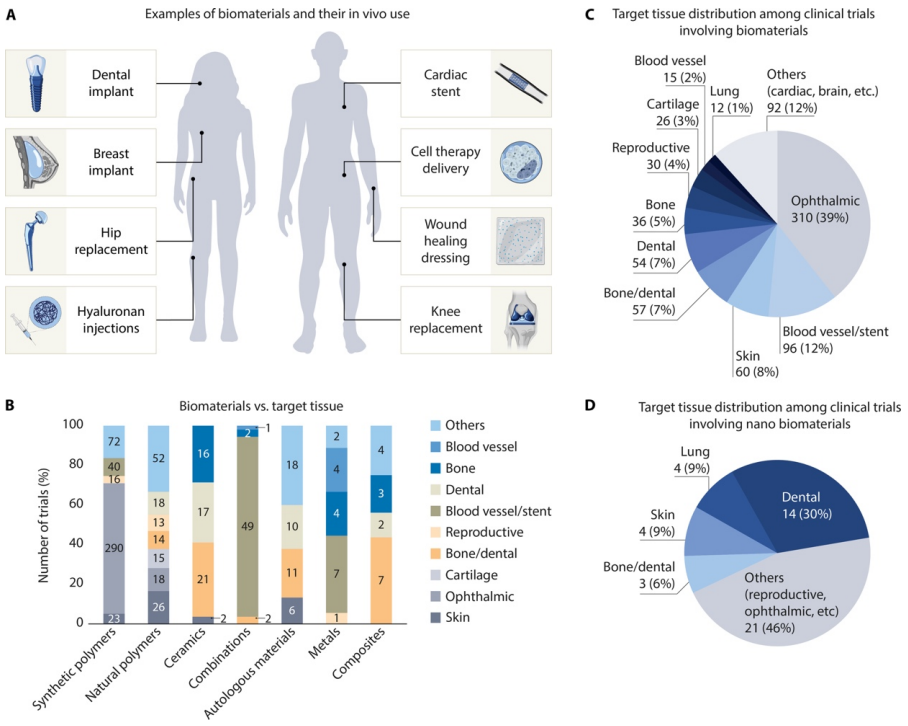


Figure 13. Clinical trials involving biomaterials in diseases and various target tissues. (**A**) The in vivo application of biomaterial in diseases and target tissues. The distribution of clinical trials involving biomaterials in (**B**) disease categories and (**C**) various target tissues. (**D**) The distribution of clinical trials involving nanobiomaterials in different target tissues. Reproduced from ref. [203]. This is an open-access article distributed under the terms of the Creative Commons Attribution-NonCommercial license, https://creativecommons.org/licenses/by-nc/4.0/ (accessed on 1 November 2024).

Tissue-engineered constructs have been successfully utilized in the repair of skin, bladder, bones, and cartilage [7]. Engineered tissue constructs can be assembled from primary cells or specific tissue culture lines: fibroblasts, endothelial cells, or cardiac muscle [204]. However, tissue constructs may not be able to seamlessly mimic the biological tissue due to differences in structure, organization, and lower cell density [204]. This gives rise to functional differences. Tissue engineering constructs also require a continued blood supply for long-term stability following implantation [205]. Thus, a continuing goal is to develop engineered tissue constructs with mechanical, structural, and functional properties that mimic biological tissue function and provide cues to diverse intercellular interactions.

Chronic wound healing is another area of regenerative medicine, currently undergoing clinical trials. Advanced wound care approaches, such as stem cells, biomaterials, and innovative treatment techniques are integrated to promote tissue regeneration and healing. However, there have been limited clinical case studies for bone tissue engineering using scaffolds and osteogenic cells, pointing to the slow advances in clinical tissue engineering [9,206]. Tissue rejection, challenges in surgical reconstruction, and lack of donor tissues are some of the major drawbacks that may impair the integration of inorganic biomaterials with natural tissues or organs to drive cell differentiation. Further, scalability, cost, regulatory issues, and uptake are other factors that largely limit the clinical translation of complex structures [207,208]. Also, ethical concerns concerning the utilization of tissue cells and human embryonic stem cells cannot be sidelined. Thus, clinical translation of regenerative medicine requires the development of appropriate guidelines for the safe and effective delivery of regenerative medicine strategies. The involvement of start-up corporations and enterprises is essential for streamlining the development of innovative therapies, and the speedy and effective delivery of regenerative medicine to physicians and patients [209]. These advances are pivotal in disseminating cutting-edge research and

facilitating clinical applications. By bridging the gap between laboratory research and practical implementation, we can ensure that advancements in regenerative medicine reach those in need more swiftly and effectively.

5. Conclusions

Regenerative medicine and tissue engineering integrate engineering, materials science, clinical translation, stem cell science, and biology to promote the regeneration of diseased tissues and the formation of new tissues and organ systems. Advances in regenerative engineering have significantly improved the management of traumatic patients requiring organ replacement and/or repair, while also promoting the development of biological substitutes for diseased or damaged tissues. These innovations offer renewed hope for augmenting patient recovery and long-term outcomes in severe injury, trauma, or chronic situations. The review offers a detailed overview of the recent advancements, developments, and applications of inorganic nanoparticles and biomaterials in tissue engineering and regenerative therapy. At the intersection of biomaterial science and nanotechnology, inorganic biomaterials are extensively being studied for diagnostic, imaging, therapeutic delivery applications, and regenerative medicine. Development of inorganic biomaterials to stimulate new cells and regenerative tissue involves a detailed understanding of (1) fabrication techniques, (2) development of composition, morphology, and functionality, and (3) optimizing the mechanical and bioactive properties to obtain the desired function. Technical advances have facilitated the fabrication of engineered tissue constructs and tailor-made grafts that mimic natural tissue. Given the complexity of tissue engineering procedures, interdisciplinary collaboration between engineers, scientists, biologists, and clinical specialists is much sought to guide novel technological advancements in regenerative medicine. This review also discusses the challenges and opportunities of combining regenerative medicine strategies with inorganic-based nanoparticles and biomaterials. The growing application of synergistic strategies in regenerative medicine offers a promising opportunity to integrate advanced techniques, applications, and prospects for use in clinical trials and modern healthcare.

Funding: This research received no external funding.

Conflicts of Interest: The author has no conflicts of interest.

References

1. Mao, A.S.; Mooney, D.J. Regenerative Medicine: Current Therapies and Future Directions. *Proc. Natl. Acad. Sci. USA* **2015**, *112*, 14452. [CrossRef] [PubMed]
2. Mason, C.; Dunnill, P. A Brief Definition of Regenerative Medicine. *Regen. Med.* **2008**, *3*, 1. [CrossRef] [PubMed]
3. Jin, Y.; Li, S.; Yu, Q.; Chen, T.; Liu, D. Application of Stem Cells in Regeneration Medicine. *MedComm* **2023**, *4*, e291. [CrossRef] [PubMed]
4. McKinley, K.L.; Longaker, M.T.; Naik, S. Emerging Frontiers in Regenerative Medicine. *Science* **2023**, *380*, 796. [CrossRef]
5. Bianchi, E.; Vigani, B.; Viseras, C.; Ferrari, F.; Rossi, S.; Sandri, G. Inorganic Nanomaterials in Tissue Engineering. *Pharmaceutics* **2022**, *14*, 1127. [CrossRef]
6. Salgado, A.J.; Oliveira, J.M.; Martins, A.; Teixeira, F.G.; Silva, N.A.; Neves, N.M.; Sousa, N.; Reis, R.L. Chapter One—Tissue Engineering and Regenerative Medicine: Past, Present, and Future. *Int. Rev. Neurobiol. Acad. Press* **2013**, *108*, 1. [CrossRef]
7. O'Brien, F.J. Biomaterials & Scaffolds For Tissue Engineering. *Mater. Today* **2011**, *14*, 88. [CrossRef]
8. Vishwakarma, A.; Sharpe, P.; Shi, S.; Ramalingam, M. Chapter 1—An Introduction to Stem Cell Biology and Tissue Engineering. In *Stem Cell Biology and Tissue Engineering in Dental Sciences*; Academic Press: Cambridge, MA, USA, 2015; Volume 1. [CrossRef]
9. Ikada, Y. Challenges in Tissue Engineering. *J. Royal Soc. Interface* **2006**, *3*, 589. [CrossRef]
10. Wang, Y.; Zhang, W.; Yao, Q. Copper-based Biomaterials for Bone and Cartilage Tissue Engineering. *J. Orthop. Translat.* **2021**, *29*, 60. [CrossRef]
11. Yun, Y.R.; Won, J.E.; Jeon, E.; Lee, S.; Kang, W.; Jo, H.; Jang, J.H.; Shin, U.S.; Kim, H.W. Fibroblast Growth Factors: Biology, Function, and Application For Tissue Regeneration. *J. Tissue Eng.* **2010**, 218142. [CrossRef]
12. Sheikh, Z.; Javaid, M.A.; Hamdan, N.; Hashmi, R. Bone Regeneration Using Bone Morphogenetic Proteins and Various Biomaterial Carriers. *Materials* **2015**, *8*, 1778. [CrossRef] [PubMed]
13. Katagiri, T.; Watabe, T. Bone Morphogenetic Proteins. *Cold Spring Harb. Perspect. Biol.* **2016**, *8*, a021899. [CrossRef] [PubMed]

14. Lademann, F.; Hofbauer, L.C.; Rauner, M. The Bone Morphogenetic Protein Pathway: The Osteoclastic Perspective. *Front. Cell Dev. Biol.* **2020**, *8*, 586031. [CrossRef] [PubMed]
15. Kulikauskas, M.R.; Shaka, X.; Bautch, V.L. The Versatility and Paradox of BMP Signaling in Endothelial Cell Behaviors and Blood Vessel Function. *Cell Mol. Life Sci.* **2022**, *79*, 77. [CrossRef]
16. Zakrzewski, W.; Dobrzyński, M.; Szymonowicz, M.; Rybak, Z. Stem Cells: Past, Present, and Future. *Stem Cell Res. Ther.* **2019**, *10*, 68. [CrossRef]
17. Kolios, G.; Moodley, Y. Introduction to Stem Cells and Regenerative Medicine. *Respiration* **2013**, *85*, 3. [CrossRef]
18. Abdal Dayem, A.M.; Saadeldin, I.M.; Zhang, S. Editorial: Crosslinking ROS signaling and stem cells. *Front. Cell Dev. Biol.* **2022**, *10*, 1101802. [CrossRef]
19. Amini, A.R.; Laurencin, C.T.; Nukavarapu, S.P. Bone Tissue Engineering: Recent Advances and Challenges. *Crit. Rev. Biomed. Eng.* **2012**, *40*, 363. [CrossRef]
20. Zhang, C.P.; Fu, X.B. Therapeutic Potential of Stem Cells in Skin Repair and Regeneration. *Chin. J. Traumatol.* **2008**, *11*, 209. [CrossRef]
21. Zhang, W.; Huang, X. Stem Cell-Based Drug Delivery Strategy For Skin Regeneration and Wound Healing: Potential Clinical Applications. *Inflamm. Regen.* **2023**, *43*, 33. [CrossRef]
22. Duscher, D.; Barrera, J.; Wong, V.W.; Maan, Z.N.; Whittam, A.J.; Januszyk, M.; Gurtner, G.C. Stem Cells in Wound Healing: The Future of Regenerative Medicine? A Mini-Review. *Gerontology* **2016**, *62*, 216. [CrossRef] [PubMed]
23. Hoang, D.M.; Pham, P.T.; Bach, T.Q.; Ngo, A.T.; Nguyen, Q.T.; Phan, T.T.; Nguyen, G.H.; Le, P.T.; Hoang, V.T.; Forsyth, N.R.; et al. Stem Cell-Based Therapy For Human Diseases. *Signal Transduct. Target. Ther.* **2022**, *7*, 272. [CrossRef] [PubMed]
24. Rajabzadeh, N.; Fathi, E.; Farahzadi, R. Stem Cell-Based Regenerative Medicine. *Stem Cell Investig.* **2019**, *6*, 19. [CrossRef] [PubMed]
25. Tabansky, I.; Stern, J.N.H. Basics of Stem Cell Biology as Applied to the Brain. In *Stem Cells in Neuroendocrinology*; Pfaff, D., Christen, Y., Eds.; Springer: Cham, Switzerland, 2016; pp. 11–24.
26. Harris, D.T.; Badowski, M.; Ahmad, N.; Gaballa, M.A. The potential of Cord Blood Stem Cells for use in Regenerative Medicine. *Expert Opin. Biol. Ther.* **2007**, *7*, 1311. [CrossRef] [PubMed]
27. Devi, S.; Bongale, A.M.; Tefera, M.A.; Dixit, P.; Bhanap, P. Fresh Umbilical Cord Blood-A Source of Multipotent Stem Cells, Collection, Banking, Cryopreservation, and Ethical Concerns. *Life* **2023**, *13*, 1794. [CrossRef]
28. Sanchez-Petitto, G.; Rezvani, K.; Daher, M.; Rafei, H.; Kebriaei, P.; Shpall, E.J.; Olson, A. Umbilical Cord Blood Transplantation: Connecting Its Origin to Its Future. *Stem Cells Transl. Med.* **2023**, *12*, 55. [CrossRef]
29. Barker, J.N.; Byam, C.E.; Kernan, N.A.; Lee, S.S.; Hawke, R.M.; Doshi, K.A.; Wells, D.S.; Heller, G.; Papadopoulos, E.B.; Scaradavou, A.; et al. Availability of Cord Blood Extends Allogeneic Hematopoietic Stem Cell Transplant Access to Racial and Ethnic Minorities. *Biol. Blood Marrow Transpl.* **2010**, *16*, 1541. [CrossRef]
30. Gragert, L.; Eapen, M.; Williams, E.; Freeman, J.; Spellman, S.; Baitty, R.; Hartzman, R.; Rizzo, J.D.; Horowitz, M.; Confer, D.; et al. HLA Match Likelihoods For Hematopoietic Stem-Cell Grafts in the U.S. Registry. *N. Engl. J. Med.* **2014**, *371*, 339. [CrossRef]
31. Weiss, M.L.; Troyer, D.L. Stem Cells in the Umbilical Cord. *Stem Cell Rev.* **2006**, *2*, 155. [CrossRef]
32. Kurtzberg, J.; Lyerly, A.D.; Sugarman, J. Untying the Gordian Knot: Policies, Practices, and Ethical Issues Related to Banking of Umbilical Cord Blood. *J. Clin. Investig.* **2005**, *115*, 2592. [CrossRef]
33. Hoover-Plow, J.; Gong, Y. Challenges For Heart Disease Stem Cell Therapy. *Vasc. Health Risk Manag.* **2012**, *8*, 99. [CrossRef] [PubMed]
34. Mohr, A.; Zwacka, R. The Future of Mesenchymal Stem Cell-Based Therapeutic Approaches For Cancer—From Cells to Ghosts. *Cancer Lett.* **2018**, *414*, 239. [CrossRef] [PubMed]
35. Chen, F.; Zhao, E.R.; Hableel, G.; Hu, T.; Kim, T.; Li, J.; Gonzalez-Pech, N.I.; Cheng, D.J.; Lemaster, J.E.; Xie, Y.; et al. Increasing the Efficacy of Stem Cell Therapy via Triple-Function Inorganic Nanoparticles. *ACS Nano* **2019**, *13*, 6605. [CrossRef]
36. Nourian Dehkordi, A.; Mirahmadi Babaheydari, F.; Chehelgerdi, M.; Raeisi Dehkordi, S. Skin Tissue Engineering: Wound Healing Based on Stem-Cell-Based Therapeutic Strategies. *Stem Cell Res. Ther.* **2019**, *10*, 111. [CrossRef] [PubMed]
37. Butler, K.L.; Goverman, J.; Ma, H.; Fischman, A.; Yu, Y.M.; Bilodeau, M.; Rad, A.M.; Bonab, A.A.; Tompkins, R.G.; Fagan, S.P. Stem Cells and Burns: Review and Therapeutic Implications. *J. Burn Care Res.* **2010**, *31*, 874. [CrossRef] [PubMed]
38. Chu, G.Y.; Chen, Y.F.; Chen, H.Y.; Chan, M.H.; Gau, C.S.; Weng, S.M. Stem Cell Therapy on Skin: Mechanisms, Recent Advances and Drug Reviewing Issues. *J. Food Drug Anal.* **2018**, *26*, 14. [CrossRef]
39. Ojeh, N.; Pastar, I.; Tomic-Canic, M.; Stojadinovic, O. Cells in Skin Regeneration, Wound Healing, and Their Clinical Applications. *Int. J. Mol. Sci.* **2015**, *16*, 25476. [CrossRef]
40. Díaz-García, D.; Filipová, A.; Garza-Veloz, I.; Martinez-Fierro, M.L. A Beginner's Introduction to Skin Stem Cells and Wound Healing. *Int. J. Mol. Sci.* **2021**, *22*, 11030. [CrossRef]
41. Gurtner, G.C.; Werner, S.; Barrandon, Y.; Longaker, M.T. Wound Repair and Regeneration. *Nature* **2008**, *453*, 314. [CrossRef]
42. Clevers, H. Wnt/Beta-Catenin Signaling in Development and Disease. *Cell* **2006**, *127*, 469. [CrossRef]
43. Logan, C.Y.; Nusse, R. The Wnt Signaling Pathway in Development and Disease. *Annu. Rev. Cell Dev. Biol.* **2004**, *20*, 781. [CrossRef] [PubMed]
44. Holland, J.D.; Klaus, A.; Garratt, A.N.; Birchmeier, W. Wnt Signaling in Stem and Cancer Stem Cells. *Curr. Opin. Cell Biol.* **2013**, *25*, 254. [CrossRef] [PubMed]

45. Tottoli, E.M.; Dorati, R.; Genta, I.; Chiesa, E.; Pisani, S.; Conti, B. Skin Wound Healing Process and New Emerging Technologies for Skin Wound Care and Regeneration. *Pharmaceutics* **2020**, *12*, 735. [CrossRef] [PubMed]
46. Khaled, M.M.; Ibrahium, A.M.; Abdelgalil, A.I.; El-Saied, M.A.; El-Bably, S.H. Regenerative Strategies in Treatment of Peripheral Nerve Injuries in Different Animal Models. *Tissue Eng. Regen. Med.* **2023**, *20*, 839. [CrossRef]
47. Frausin, S.; Viventi, S.; Verga Falzacappa, L.; Quattromani, M.J.; Leanza, G.; Tommasini, A.; Valencic, E. Wharton's Jelly Derived Mesenchymal Stromal Cells: Biological Properties, Induction of Neuronal Phenotype and Current Applications in Neurodegeneration Research. *Acta Histochem.* **2015**, *117*, 329. [CrossRef]
48. Seyed-Forootan, K.; Karimi, H.; Jafarian, A.-A.; Seyed-Forootan, N.-S.; Ravari, F.K.; Karimi, A.-M. Nerve Regeneration and Stem Cells. *Biomed. J. Sci.Tech. Res.* **2019**, *18*, 13540. [CrossRef]
49. Pan, M.; Wang, X.; Chen, Y.; Cao, S.; Wen, J.; Wu, G.; Li, Y.; Li, L.; Qian, C.; Qin, Z.; et al. Tissue Engineering With Peripheral Blood-Derived Mesenchymal Stem Cells Promotes the Regeneration of Injured Peripheral Nerves. *Exp. Neurol.* **2017**, *292*, 92. [CrossRef]
50. Zhang, R.C.; Du, W.Q.; Zhang, J.Y.; Yu, S.X.; Lu, F.Z.; Ding, H.M.; Cheng, Y.B.; Ren, C.; Geng, D.Q. Mesenchymal Stem Cell Treatment For Peripheral Nerve Injury: A Narrative Review. *Neural Regen. Res.* **2021**, *16*, 2170. [CrossRef]
51. Yi, S.; Zhang, Y.; Gu, X.; Huang, L.; Zhang, K.; Qian, T.; Gu, X. Application of Stem Cells in Peripheral Nerve Regeneration. *Burns. Trauma* **2020**, *8*, tkaa002. [CrossRef]
52. Zeng, C.W.; Zhang, C.L. Neuronal Regeneration After Injury: A New Perspective on Gene Therapy. *Front. Neurosci.* **2023**, *17*, 1181816. [CrossRef]
53. Zang, X.; Song, J.; Li, Y.; Han, Y. Targeting Necroptosis as an Alternative Strategy in Tumor Treatment: From Drugs to Nanoparticles. *J. Control Release* **2022**, *349*, 213. [CrossRef] [PubMed]
54. Spirescu, V.A.; Chircov, C.; Grumezescu, A.M.; Vasile, B.Ș.; Andronescu, E. Inorganic Nanoparticles and Composite Films for Antimicrobial Therapies. *Int. J. Mol. Sci.* **2021**, *22*, 4595. [CrossRef] [PubMed]
55. Kim, D.; Kim, J.; Park, Y.I.; Lee, N.; Hyeon, T. Recent Development of Inorganic Nanoparticles for Biomedical Imaging. *ACS Cent. Sci.* **2018**, *4*, 324. [CrossRef] [PubMed]
56. Alshammari, B.H.; Lashin, M.M.; Mahmood, M.A.; Al-Mubaddel, F.S.; Ilyas, N.; Rahman, N.; Sohail, M.; Khan, A.; Abdullaev, S.S.; Khan, R. Organic and Inorganic Nanomaterials: Fabrication, Properties and Applications. *RSC Adv.* **2023**, *13*, 13735. [CrossRef]
57. Giljohann, D.A.; Seferos, D.S.; Daniel, W.L.; Massich, M.D.; Patel, P.C.; Mirkin, C.A. Gold Nanoparticles for Biology and Medicine. *Angew. Chem. Int. Ed. Engl.* **2010**, *49*, 3280. [CrossRef]
58. Ma, X.; Luan, Z.; Li, J. Inorganic Nanoparticles-Based Systems in Biomedical Applications of Stem Cells: Opportunities and Challenges. *Int. J. Nanomed.* **2023**, *18*, 143. [CrossRef]
59. Zheng, Y.; Wu, J.; Zhu, Y.; Wu, C. Inorganic-Based Biomaterials for Rapid Hemostasis and Wound Healing. *Chem. Sci.* **2022**, *14*, 29. [CrossRef]
60. Ma, J.; Wu, C. Bioactive Inorganic Particles-Based Biomaterials for Skin Tissue Engineering. *Exploration* **2022**, *2*, 20210083. [CrossRef]
61. Dalisson, B.; Barralet, J. Bioinorganics and Wound Healing. *Adv. Healthc. Mater.* **2019**, *8*, e1900764. [CrossRef]
62. Anselmo, A.C.; Mitragotri, S. A Review of Clinical Translation of Inorganic Nanoparticles. *AAPS J.* **2015**, *17*, 1041. [CrossRef]
63. Zheng, X.; Zhang, P.; Fu, Z.; Meng, S.; Dai, L.; Yang, H. Applications of Nanomaterials in Tissue Engineering. *RSC Adv.* **2021**, *11*, 19041. [CrossRef] [PubMed]
64. Brokesh, A.M.; Gaharwar, A.K. Inorganic Biomaterials for Regenerative Medicine. *ACS Appl. Mater. Interfaces* **2020**, *12*, 5319. [CrossRef] [PubMed]
65. Gao, Y.; Wang, X.; Fan, C. Advances in Graphene-Based 2D Materials for Tendon, Nerve, Bone/Cartilage Regeneration and Biomedicine. *iScience* **2024**, *27*, 110214. [CrossRef] [PubMed]
66. Arora, P.; Sindhu, A.; Dilbaghi, N.; Chaudhury, A.; Rajakumar, G.; Rahuman, A.A. Nano-Regenerative Medicine Towards Clinical Outcome of Stem Cell and Tissue Engineering in Humans. *J. Cell Mol. Med.* **2012**, *16*, 1991. [CrossRef]
67. Kim, Y.-H.; Vijayavenkataraman, S.; Cidonio, G. Biomaterials and Scaffolds for Tissue Engineering and Regenerative Medicine. *BMC Methods* **2024**, *1*, 2. [CrossRef]
68. Chan, B.P.; Leong, K.W. Scaffolding in Tissue Engineering: General Approaches and Tissue-Specific Considerations. *Eur. Spine J.* **2008**, *17* (Suppl. S4), 467. [CrossRef]
69. Krishani, M.; Shin, W.Y.; Suhaimi, H.; Sambudi, N.S. Development of Scaffolds from Bio-Based Natural Materials for Tissue Regeneration Applications: A Review. *Gels* **2023**, *9*, 100. [CrossRef]
70. Mitchell, M.J.; Billingsley, M.M.; Haley, R.M.; Wechsler, M.E.; Peppas, N.A.; Langer, R. Engineering Precision Nanoparticles for Drug Delivery. *Nat. Rev. Drug Discov.* **2021**, *20*, 101. [CrossRef]
71. Raju, G.S.R.; Dariya, B.; Mungamuri, S.K.; Chalikonda, G.; Kang, S.M.; Khan, I.N.; Sushma, P.S.; Nagaraju, G.P.; Pavitra, E.; Han, Y.K. Nanomaterials Multifunctional Behavior For Enlightened Cancer Therapeutics. *Semin. Cancer Biol.* **2021**, *69*, 178. [CrossRef]
72. Zheng, J.J.; Jiang, X.C.; Li, Y.S.; Gao, J.Q. Inorganic Nanoparticle-Integrated Mesenchymal Stem Cells: A Potential Biological Agent For Multifaceted Applications. *MedComm* **2023**, *4*, e313. [CrossRef]
73. Devin, J.E.; Attawia, M.A.; Laurencin, C.T. Three-Dimensional Degradable Porous Polymer-Ceramic Matrices For Use in Bone Repair. *J. Biomater. Sci. Polym. Ed.* **1996**, *7*, 661. [CrossRef] [PubMed]

74. Blokhuis, T.J.; Arts, J.J. Bioactive and Osteoinductive Bone Graft Substitutes: Definitions, Facts and Myths. *Injury* **2011**, *42*, S26. [CrossRef] [PubMed]
75. Hasan, A.; Morshed, M.; Memic, A.; Hassan, S.; Webster, T.J.; Marei, H.E. Nanoparticles in Tissue Engineering: Applications, Challenges and Prospects. *Int. J. Nanomed.* **2018**, *13*, 5637. [CrossRef] [PubMed]
76. Antony, S.A.; Anju, T.R.; Thomas, B. Nature-Inspired Biomimetic Polymeric Materials and Their Applications. In *Handbook of Biopolymers*; Thomas, S., AR, A., Jose Chirayil, C., Thomas, B., Eds.; Springer: Singapore, 2022. [CrossRef]
77. Kučuk, N.; Primožič, M.; Knez, Ž.; Leitgeb, M. Sustainable Biodegradable Biopolymer-Based Nanoparticles for Healthcare Applications. *Int. J. Mol. Sci.* **2023**, *24*, 3188. [CrossRef]
78. Park, S.; Rahaman, K.A.; Kim, Y.C.; Jeon, H.; Han, H.S. Fostering Tissue Engineering and Regenerative Medicine to Treat Musculoskeletal Disorders in Bone and Muscle. *Bioact. Mater.* **2024**, *40*, 345. [CrossRef]
79. Zhang, Q.; Xiao, L.; Xiao, Y. Porous Nanomaterials Targeting Autophagy in Bone Regeneration. *Pharmaceutics* **2021**, *13*, 1572. [CrossRef]
80. Malvindi, M.A.; De Matteis, V.; Galeone, A.; Brunetti, V.; Anyfantis, G.C.; Athanassiou, A.; Cingolani, R.; Pompa, P.P. Toxicity Assessment of Silica Coated Iron Oxide Nanoparticles and Biocompatibility Improvement by Surface Engineering. *PLoS ONE* **2014**, *9*, e85835. [CrossRef]
81. Di Bucchianico, S.; Cappellini, F.; Le Bihanic, F.; Zhang, Y.; Dreij, K.; Karlsson, H.L. Genotoxicity of TiO_2 Nanoparticles Assessed by Mini-Gel Comet Assay and Micronucleus Scoring with Flow Cytometry. *Mutagenesis* **2017**, *32*, 127. [CrossRef]
82. Santonastaso, M.; Mottola, F.; Colacurci, N.; Iovine, C.; Pacifico, S.; Cammarota, M.; Cesaroni, F.; Rocco, L. In vitro Genotoxic Effects of Titanium Dioxide Nanoparticles (n-TiO_2) in Human Sperm Cells. *Mol. Reprod. Dev.* **2019**, *86*, 1369. [CrossRef]
83. Chen, T.; Yan, J.; Li, Y. Genotoxicity of Titanium Dioxide Nanoparticles. *J. Food Drug Anal.* **2014**, *22*, 95. [CrossRef]
84. Manzoor, Q.; Sajid, A.; Ali, Z.; Nazir, A.; Sajid, A.; Imtiaz, F.; Iqbal, S.; Younas, U.; Arif, H.; Iqbal, M. Toxicity Spectrum and Detrimental Effects of Titanium Dioxide Nanoparticles as an Emerging Pollutant: A Review. *Desalination Water Treat.* **2024**, *317*, 100025. [CrossRef]
85. Saquib, Q.; Al-Khedhairy, A.A.; Siddiqui, M.A.; Abou-Tarboush, F.M.; Azam, A.; Musarrat, J. Titanium Dioxide Nanoparticles Induced Cytotoxicity, Oxidative Stress and DNA Damage in Human Amnion Epithelial (WISH) Cells. *Toxicol. Vitro* **2012**, *26*, 351. [CrossRef] [PubMed]
86. Fattori, A.C.; Brassolatti, P.; Feitosa, K.A.; Gonçalves, M.P.; Correia, R.D.; Albuquerque, Y.R.; Rodolpho, J.M.; Luna, G.L.; Bernardi, J.C.; Zucolotto, V.; et al. Titanium Dioxide Nanoparticle (TiO_2 NP) Induces Toxic Effects on LA-9 Mouse Fibroblast Cell Line. *Cell Physiol. Biochem.* **2023**, *57*, 63. [CrossRef] [PubMed]
87. Jin, C.Y.; Zhu, B.S.; Wang, X.F.; Lu, Q.H. Cytotoxicity of Titanium Dioxide Nanoparticles in Mouse Fibroblast Cells. *Chem. Res. Toxicol.* **2008**, *21*, 1871. [CrossRef]
88. Afşar, O.; Oltulu, Ç. Evaluation of the Cytotoxic Effect of Titanium Dioxide Nanoparticles in Human Embryonic Lung Cells. *Turk. J. Med. Sci.* **2023**, *53*, 1648. [CrossRef]
89. Gojznikar, J.; Zdravković, B.; Vidak, M.; Leskošek, B.; Ferk, P. TiO_2 Nanoparticles and Their Effects on Eukaryotic Cells: A Double-Edged Sword. *Int. J. Mol. Sci.* **2022**, *23*, 12353. [CrossRef]
90. Friggeri, G.; Moretti, I.; Amato, F.; Marrani, A.G.; Sciandra, F.; Colombarolli, S.G.; Vitali, A.; Viscuso, S.; Augello, A.; Cui, L.; et al. Multifunctional Scaffolds For Biomedical Applications: Crafting Versatile Solutions with Polycaprolactone Enriched by Graphene Oxide. *APL Bioengr.* **2024**, *8*, 016115. [CrossRef]
91. Samadian, H.; Khastar, H.; Ehterami, A.; Salehi, M. Bioengineered 3D Nanocomposite Based on Gold Nanoparticles and Gelatin Nanofibers for Bone Regeneration: In Vitro and In Vivo Study. *Sci. Rep.* **2021**, *11*, 13877. [CrossRef]
92. Samadian, H.; Zamiri, S.; Ehterami, A.; Farzamfar, S.; Vaez, A.; Khastar, H.; Alam, M.; Ai, A.; Derakhshankhah, H.; Allahyari, Z.; et al. Electrospun Cellulose Acetate/Gelatin Nanofibrous Wound Dressing Containing Berberine for Diabetic Foot Ulcer Healing: In Vitro and In Vivo Studies. *Sci. Rep.* **2020**, *10*, 8312. [CrossRef]
93. Gandhimathi, C.; Quek, Y.J.; Ezhilarasu, H.; Ramakrishna, S.; Bay, B.H.; Srinivasan, D.K. Osteogenic Differentiation of Mesenchymal Stem Cells with Silica-Coated Gold Nanoparticles for Bone Tissue Engineering. *Int. J. Mol. Sci.* **2019**, *20*, 5135. [CrossRef]
94. Wedel-Grzenda, A.; Fraczek-Szczypta, A.; Terrones, M.; Elias, A.L.; Lekka, M.; Menaszek, E.; Blazewicz, S. Polysulphone composite membranes modified with two types of carbon additives as a potential material for bone tissue regeneration. *Bull. Mater. Sci.* **2017**, *40*, 201. [CrossRef]
95. Sithole, M.N.; Kumar, P.; Du Toit, L.C.; Erlwanger, K.H.; Ubanako, P.N.; Choonara, Y.E. A 3D-Printed Biomaterial Scaffold Reinforced with Inorganic Fillers for Bone Tissue Engineering: In Vitro Assessment and In Vivo Animal Studies. *Int. J. Mol. Sci.* **2023**, *24*, 7611. [CrossRef] [PubMed]
96. Yang, L.; Rathnam, C.; Hou, Y.; Patel, M.; Cai, L.; Lee, K.-B. Rapid and Controllable Multilayer Cell Sheet Assembly via Biodegradable Nanochannel Membranes. *Adv. Funct. Mater.* **2024**, 2403367. [CrossRef]
97. Yang, L.; Chueng, S.D.; Li, Y.; Patel, M.; Rathnam, C.; Dey, G.; Wang, L.; Cai, L.; Lee, K.B. A Biodegradable Hybrid Inorganic Nanoscaffold for Advanced Stem Cell Therapy. *Nat. Commun.* **2018**, *9*, 3147. [CrossRef]
98. Baydar, S.Y.; Ay, H.F.; Cakir, R. Frontiers of Stem Cell Engineering For Nanotechnology-Mediated Drug Delivery Systems. *ADMET DMPK* **2024**, *12*, 225. [CrossRef]
99. Yang, Y.; Leong, K.W. Nanoscale Surfacing For Regenerative Medicine. *WIREs Nanomed. Nanobiotechnol.* **2010**, *2*, 478. [CrossRef]

100. Brovkina, O.; Dashinimaev, E. Advances and Complications of Regenerative Medicine in Diabetes Therapy. *PeerJ* **2020**, *8*, e9746. [CrossRef]
101. Li, D.; Liu, Y.; Wu, N. Application Progress of Nanotechnology in Regenerative Medicine of Diabetes Mellitus. *Diabetes Res. Clin. Pract.* **2022**, *190*, 109966. [CrossRef]
102. Andreadi, A.; Lodeserto, P.; Todaro, F.; Meloni, M.; Romano, M.; Minasi, A.; Bellia, A.; Lauro, D. Nanomedicine in the Treatment of Diabetes. *Int. J. Mol. Sci.* **2024**, *25*, 7028. [CrossRef]
103. Siwakoti, P.; Rennie, C.; Huang, Y.; Li, J.J.; Tuch, B.E.; McClements, L.; Xu, X. Challenges with Cell-based Therapies for Type 1 Diabetes Mellitus. *Stem Cell. Rev. Rep.* **2023**, *19*, 601. [CrossRef]
104. Yao, Y.; Ji, K.; Wang, Y.; Gu, Z.; Wang, J. Materials and Carriers Development for Glucose-Responsive Insulin. *Acc. Mater. Res.* **2022**, *3*, 960. [CrossRef]
105. Bakhru, S.H.; Furtado, S.; Morello, A.P.; Mathiowitz, E. Oral Delivery of Proteins by Biodegradable Nanoparticles. *Adv. Drug Deliv. Rev.* **2013**, *65*, 811. [CrossRef] [PubMed]
106. Rabanel, J.M.; Aoun, V.; Elkin, I.; Mokhtar, M.; Hildgen, P. Drug-Loaded Nanocarriers- Passive Targeting and Crossing of Biological Barriers. *Curr. Med. Chem.* **2012**, *19*, 3070. [CrossRef] [PubMed]
107. Veiseh, O.; Tang, B.C.; Whitehead, K.A.; Anderson, D.G.; Langer, R. Managing Diabetes with Nanomedicine: Challenges and Opportunities. *Nat. Rev. Drug Discov.* **2015**, *14*, 45. [CrossRef] [PubMed]
108. Sharma, R.; Borah, S.J.; Bhawna; Kumar, S.; Gupta, A.; Kumari, V.; Kumar, R.; Dubeyg, K.K.; Kumar, V. Emerging Trends in Nano-Based Antidiabetic Therapeutics: A Path to Effective Diabetes Management. *Mater. Adv.* **2023**, *4*, 3091. [CrossRef]
109. Liu, Y.; Zeng, S.; Ji, W.; Yao, H.; Lin, L.; Cui, H.; Santos, H.A.; Pan, G. Emerging Theranostic Nanomaterials in Diabetes and Its Complications. *Adv. Sci.* **2022**, *9*, e2102466. [CrossRef]
110. Sonomoto, K.; Yamaoka, K.; Kaneko, H.; Yamagata, K.; Sakata, K.; Zhang, X.; Kondo, M.; Zenke, Y.; Sabanai, K.; Nakayamada, S.; et al. Spontaneous Differentiation of Human Mesenchymal Stem Cells on Poly-Lactic-Co-Glycolic Acid Nano-Fiber Scaffold. *PLoS ONE* **2016**, *11*, e0153231. [CrossRef]
111. Umer, A.; Ghouri, M.D.; Muyizere, T.; Aqib, R.M.; Muhaymin, A.; Cai, R.; Chen, C. Engineered Nano-Bio Interfaces for Stem Cell Therapy. *Precis. Chem.* **2023**, *1*, 341. [CrossRef]
112. Teo, B.K.; Wong, S.T.; Lim, C.K.; Kung, T.Y.; Yap, C.H.; Ramagopal, Y.; Romer, L.H.; Yim, E.K. Nanotopography Modulates Mechanotransduction of Stem Cells and Induces Differentiation Through Focal Adhesion Kinase. *ACS Nano* **2013**, *7*, 4785. [CrossRef]
113. Ludin, A.; Gur-Cohen, S.; Golan, K.; Kaufmann, K.B.; Itkin, T.; Medaglia, C.; Lu, X.J.; Ledergor, G.; Kollet, O.; Lapidot, T. Reactive Oxygen Species Regulate Hematopoietic Stem Cell Self-Renewal, Migration and Development, as well as their Bone Marrow Microenvironment. *Antioxid. Redox Signal.* **2014**, *21*, 1605. [CrossRef]
114. Wang, C.; Liu, D.; Zhang, C.; Sun, J.; Feng, W.; Liang, X.J.; Wang, S.; Zhang, J. Defect-Related Luminescent Hydroxyapatite-Enhanced Osteogenic Differentiation of Bone Mesenchymal Stem Cells Via an ATP-Induced cAMP/PKA Pathway. *ACS Appl. Mater. Interfaces* **2016**, *8*, 11262. [CrossRef] [PubMed]
115. Przekora, A. Current Trends in Fabrication of Biomaterials for Bone and Cartilage Regeneration: Materials Modifications and Biophysical Stimulations. *Int. J. Mol. Sci.* **2019**, *20*, 435. [CrossRef]
116. Wu, Y.N.; Law, J.B.; He, A.Y.; Low, H.Y.; Hui, J.H.; Lim, C.T.; Yang, Z.; Lee, E.H. Substrate Topography Determines the Fate of Chondrogenesis from Human Mesenchymal Stem Cells Resulting in Specific Cartilage Phenotype Formation. *Nanomedicine.* **2014**, *10*, 1507. [CrossRef] [PubMed]
117. Wu, Y.N.; Yang, Z.; Hui, J.H.; Ouyang, H.W.; Lee, E.H. Cartilaginous ECM Component-Modification of the Micro-Bead Culture System For Chondrogenic Differentiation of Mesenchymal Stem Cells. *Biomaterials* **2007**, *28*, 4056. [CrossRef] [PubMed]
118. Varghese, S.; Hwang, N.S.; Canver, A.C.; Theprungsirikul, P.; Lin, D.W.; Elisseeff, J. Chondroitin Sulfate Based Niches For Chondrogenic Differentiation of Mesenchymal Stem Cells. *Matrix Biol.* **2008**, *27*, 12. [CrossRef] [PubMed]
119. Xu, H.; Akbari, M.K.; Kumar, S.; Verpoort, F.; Zhuiykov, S. Atomic layer deposition—State-of-the-art approach to nanoscale hetero-interfacial engineering of chemical sensors electrodes: A review. *Sens. Actuators B Chem.* **2021**, *331*, 129403. [CrossRef]
120. Liu, M.; Li, X.; Karuturi, S.K.; Tok, A.I.; Fan, H.J. Atomic Layer Deposition for Nanofabrication and Interface Engineering. *Nanoscale* **2012**, *4*, 1522–1528. [CrossRef]
121. Bechelany, M.; Balme, S.; Miele, P. Atomic Layer Deposition of Biobased Nanostructured Interfaces for Energy, Environmental and Health Applications. *Pure Appl. Chem.* **2015**, *87*, 751. [CrossRef]
122. Bishal, A.K.; Sukotjo, C.; Takoudis, C.G. Room Temperature TiO_2 Atomic Layer Deposition on Collagen Membrane from a Titanium Alkylamide Precursor. *J. Vacuum Sci. Technol. A.* **2017**, *35*, 01B134. [CrossRef]
123. Campoccia, D.; Montanaro, L.; Arciola, C.R. The Significance of Infection Related to Orthopedic Devices and Issues of Antibiotic Resistance. *Biomaterials* **2006**, *27*, 2331. [CrossRef]
124. Chung, C.J.; Long, H.Y. Systematic Strontium Substitution in Hydroxyapatite Coatings on Titanium via Micro-Arc Treatment and their Osteoblast/Osteoclast Responses. *Acta Biomater.* **2011**, *7*, 4081. [CrossRef] [PubMed]
125. Capek, J.; Sepúlveda, M.; Bacova, J.; Rodriguez-Pereira, J.; Zazpe, R.; Cicmancova, V.; Nyvltova, P.; Handl, J.; Knotek, P.; Baishya, K.; et al. Ultrathin TiO_2 Coatings via Atomic Layer Deposition Strongly Improve Cellular Interactions on Planar and Nanotubular Biomedical Ti Substrates. *ACS Appl. Mater. Interfaces* **2024**, *16*, 5627. [CrossRef] [PubMed]

126. Dafinone, M.I.; Feng, G.; Brugarolas, T.; Tettey, K.E.; Lee, D. Mechanical Reinforcement of Nanoparticle Thin Films Using Atomic Layer Deposition. *ACS Nano* **2011**, *5*, 5078. [CrossRef] [PubMed]
127. Saha, S.; Costa, R.C.; Silva, M.C.; Fonseca-Santos, J.M.; Chen, L.; Phakatkar, A.H.; Bhatia, H.; Faverani, L.P.; Barão, V.A.; Shokuhfar, T.; et al. Collagen Membrane Functionalized with Magnesium Oxide via Room-Temperature Atomic Layer Deposition Promotes Osteopromotive and Antimicrobial Properties. *Bioact. Mater.* **2023**, *30*, 46. [CrossRef]
128. Johnson, R.W.; Hultqvist, A.; Bent, S.F. A Brief Review of Atomic Layer Deposition: From Fundamentals to Applications. *Mater. Today* **2014**, *07*, 236–246. [CrossRef]
129. Narayan, R.J.; Adiga, S.P.; Pellin, M.J.; Curtiss, L.A.; Hryn, A.J.; Stafslien, S.; Chisholm, B.; Shih, C.C.; Shih, C.M.; Lin, S.J.; et al. Atomic Layer Deposition-Based Functionalization of Materials for Medical and Environmental Health Applications. *Philos. Trans. A Math Phys. Eng. Sci.* **2010**, *368*, 2033. [CrossRef]
130. Popov, A.M.; Lozovik, Y.E.; Fiorito, S.; Yahia, L. Biocompatibility and Applications of Carbon Nanotubes in Medical Nanorobots. *Int. J. Nanomed.* **2007**, *2*, 361.
131. Wang, J.; Huang, C.; Wang, Y.; Chen, Y.; Ding, Z.; Yang, C.; Chen, L. Exploration of the Single-Walled Carbon Nanotubes' Influence for Cartilage Repair. *Colloids Surf. A Physicochem. Eng. Asp.* **2020**, *606*, 125520. [CrossRef]
132. Szymański, T.; Semba, J.A.; Mieloch, A.A.; Cywoniuk, P.; Kempa, M.; Rybka, J.D. Hyaluronic Acid and Multiwalled Carbon Nanotubes as Bioink Additives for Cartilage Tissue Engineering. *Sci. Rep.* **2023**, *13*, 646. [CrossRef]
133. Yang, X.; Li, C.J.; Wan, Y.; Smith, P.; Shang, G.; Cui, Q. Antioxidative Fullerol Promotes Osteogenesis of Human Adipose-Derived Stem Cells. *Int. J. Nanomed.* **2014**, *9*, 4023. [CrossRef]
134. Elídóttir, K.L.; Scott, L.; Lewis, R.; Jurewicz, I. Biomimetic Approach to Articular Cartilage Tissue Engineering Using Carbon Nanotube-Coated and Textured Polydimethylsiloxane Scaffolds. *Ann. N. Y. Acad. Sci.* **2022**, *1513*, 48. [CrossRef] [PubMed]
135. Feng, Z.Q.; Yan, K.; Shi, C.; Xu, X.; Wang, T.; Li, R.; Dong, W.; Zheng, J. Neurogenic Differentiation of Adipose Derived Stem Cells on Graphene-Based Mat. *Mater. Sci. Eng. C Mater. Biol. Appl.* **2018**, *90*, 685. [CrossRef] [PubMed]
136. Rostami, F.; Tamjid, E.; Behmanesh, M. Drug-Eluting PCL/Graphene Oxide Nanocomposite Scaffolds For Enhanced Osteogenic Differentiation of Mesenchymal Stem Cells. *Mater. Sci. Eng. C Mater. Biol. Appl.* **2020**, *115*, 111102. [CrossRef]
137. Wei, S.; Zou, L.; Hu, X.; Li, Q. Carbon Nanomaterials in the Treatment of Infectious Bone Defects and Wound Scars after Wushu Fractures. *J. Chem.* **2020**, 2094273. [CrossRef]
138. Shen, Y.; Wu, L.; Qin, D.; Xia, Y.; Zhou, Z.; Zhang, X.; Wu, X. Carbon Black Suppresses the Osteogenesis of Mesenchymal Stem Cells: The Role of Mitochondria. *Part Fibre Toxicol.* **2018**, *15*, 16. [CrossRef]
139. Zheng, S.; Tian, Y.; Ouyang, J.; Shen, Y.; Wang, X.; Luan, J. Carbon Nanomaterials for Drug Delivery and Tissue Engineering. *Front. Chem.* **2022**, *10*, 990362. [CrossRef]
140. Holmannova, D.; Borsky, P.; Svadlakova, T.; Borska, L.; Fiala, Z. Carbon Nanoparticles and Their Biomedical Applications. *Appl. Sci.* **2022**, *12*, 7865. [CrossRef]
141. Li, L.; Zhu, Z.; Xiao, W.; Li, L. Multi-Walled Carbon Nanotubes Promote Cementoblast Differentiation and Mineralization through the TGF-β/Smad Signaling Pathway. *Int. J. Mol. Sci.* **2015**, *16*, 3188. [CrossRef]
142. Saleemi, M.A.; Hosseini Fouladi, M.; Yong, P.V.C.; Chinna, K.; Palanisamy, N.K.; Wong, E.H. Toxicity of Carbon Nanotubes: Molecular Mechanisms, Signaling Cascades, and Remedies in Biomedical Applications. *Chem. Res. Toxicol.* **2021**, *34*, 24. [CrossRef]
143. Liu, Y.; Zhao, Y.; Sun, B.; Chen, C. Understanding the Toxicity of Carbon Nanotubes. *Acc. Chem. Res.* **2013**, *46*, 702. [CrossRef]
144. Hu, W.; Peng, C.; Lv, M.; Li, X.; Zhang, Y.; Chen, N.; Fan, C.; Huang, Q. Protein Corona-Mediated Mitigation of Cytotoxicity of Graphene Oxide. *ACS Nano* **2011**, *5*, 3693. [CrossRef] [PubMed]
145. Eivazzadeh-Keihan, R.; Maleki, A.; de la Guardia, M.; Bani, M.S.; Chenab, K.K.; Pashazadeh-Panahi, P.; Baradaran, B.; Mokhtarzadeh, A.; Hamblin, M.R. Carbon Based Nanomaterials for Tissue Engineering of Bone: Building New Bone on Small Black Scaffolds: A Review. *J. Adv. Res.* **2019**, *18*, 185. [CrossRef] [PubMed]
146. Yuan, X.; Zhang, X.; Sun, L.; Wei, Y.; Wei, X. Cellular Toxicity and Immunological Effects of Carbon-based Nanomaterials. *Part Fibre Toxicol.* **2019**, *16*, 18. [CrossRef]
147. Peng, Z.; Liu, X.; Zhang, W.; Zeng, Z.; Liu, Z.; Zhang, C.; Liu, Y.; Shao, B.; Liang, Q.; Tang, W.; et al. Advances in the Application, Toxicity and Degradation of Carbon Nanomaterials in Environment: A Review. *Environ. Int.* **2020**, *134*, 105298. [CrossRef] [PubMed]
148. De Luca, S.; Verdoliva, V.; Kargozar, S.; Baino, F. Bioactive Glass-Ceramic Scaffolds Coated with Hyaluronic Acid-Fatty Acid Conjugates: A Feasibility Study. *J. Funct. Biomater.* **2023**, *14*, 26. [CrossRef]
149. Cannio, M.; Bellucci, D.; Roether, J.A.; Boccaccini, D.N.; Cannillo, V. Bioactive Glass Applications: A Literature Review of Human Clinical Trials. *Materials* **2021**, *14*, 5440. [CrossRef]
150. Sergi, R.; Bellucci, D.; Cannillo, V. A Review of Bioactive Glass/Natural Polymer Composites: State of the Art. *Materials* **2020**, *13*, 5560. [CrossRef]
151. El-Rashidy, A.A.; Roether, J.A.; Harhaus, L.; Kneser, U.; Boccaccini, A.R. Regenerating Bone with Bioactive Glass Scaffolds: A Review of in vivo Studies in Bone Defect Models. *Acta Biomater.* **2017**, *62*, 1–28. [CrossRef]
152. Fiume, E.; Barberi, J.; Verné, E.; Baino, F. Bioactive Glasses: From Parent 45S5 Composition to Scaffold-Assisted Tissue-Healing Therapies. *J. Funct. Biomater.* **2018**, *9*, 24. [CrossRef]
153. Hench, L.L. The Story of Bioglass. *J. Mater. Sci. Mater. Med.* **2006**, *17*, 967. [CrossRef]

154. Gerhardt, L.C.; Boccaccini, A.R. Bioactive Glass and Glass-Ceramic Scaffolds for Bone Tissue Engineering. *Materials* **2010**, *3*, 3867. [CrossRef] [PubMed]
155. Jones, J.R.J. Bioactive Ceramics and Glasses. In *Tissue Engineering Using Ceramics and Polymers*, 1st ed.; Boccaccini, A.R., Gough, J., Eds.; Woodhead Publishing Limited CRC Press: Cambridge, UK, 2007; Volume 1, pp. 52–71.
156. Pajares-Chamorro, N.; Chatzistavrou, X. Bioactive Glass Nanoparticles for Tissue Regeneration. *ACS Omega* **2020**, *5*, 12716. [CrossRef] [PubMed]
157. Dreanca, A.; Bogdan, S.; Popescu, A.; Sand, D.; Pall, E.; Astilean, A.N.; Pestean, C.; Toma, C.; Marza, S.; Taulescu, M.; et al. The Evaluation of the Osteopromoting Capabilities of Composites Based on Biopolymers and Gold/Silver Nanoparticles Doped Bioactive Glasses on an Experimental Rat Bone Defect. *Biomed. Mater.* **2023**, *18*. [CrossRef] [PubMed]
158. Niu, W.; Chen, M.; Guo, Y.; Wang, M.; Luo, M.; Cheng, W.; Wang, Y.; Lei, B. A Multifunctional Bioactive Glass-Ceramic Nanodrug for Post-Surgical Infection/Cancer Therapy-Tissue Regeneration. *ACS Nano* **2021**, *15*, 14323. [CrossRef] [PubMed]
159. Khatami, N.; Khoshfetrat, A.B.; Khaksar, M.; Zamani, A.R.N.; Rahbarghazi, R. Collagen-Alginate-Nano-Silica Microspheres Improved the Osteogenic Potential of Human Osteoblast-Like MG-63 Cells. *J. Cell Biochem.* **2019**, *120*, 15069. [CrossRef]
160. Mostafa, A.A.; El-Sayed, M.M.H.; Emam, A.N.; Abd-Rabou, A.A.; Dawood, R.M.; Oudadesse, H. Bioactive Glass Doped with Noble Metal Nanoparticles for Bone Regeneration: In vitro Kinetics and Proliferative Impact on Human Bone Cell Line. *RSC Adv.* **2021**, *11*, 25628. [CrossRef]
161. Zengin, A.; Castro, J.P.O.; Habibovic, P.; van Rijt, S.H. Injectable, Self-Healing Mesoporous Silica Nanocomposite Hydrogels with Improved Mechanical Properties. *Nanoscale* **2021**, *13*, 1144. [CrossRef]
162. Hou, X.; Zhang, L.; Zhou, Z.; Luo, X.; Wang, T.; Zhao, X.; Lu, B.; Chen, F.; Zheng, L. Calcium Phosphate-Based Biomaterials for Bone Repair. *J. Funct. Biomater.* **2022**, *13*, 187. [CrossRef]
163. Xiao, D.; Zhang, J.; Zhang, C.; Barbieri, D.; Yuan, H.; Moroni, L.; Feng, G. The Role of Calcium Phosphate Surface Structure in Osteogenesis and the Mechanisms Involved. *Acta Biomater.* **2020**, *106*, 22. [CrossRef]
164. Zhi, H.; Qingling, F.; Bo, Y.; Songjian, L. Biomimetic Properties of an Injectable Chitosan/Nano-Hydroxyapatite/Collagen Composite. *Mater. Sci. Eng. C* **2011**, *31*, 683. [CrossRef]
165. Shibuya, S.; Ozawa, Y.; Watanabe, K.; Izuo, N.; Toda, T.; Yokote, K.; Shimizu, T. Palladium and Platinum Nanoparticles Attenuate Aging-Like Skin Atrophy via Antioxidant Activity in Mice. *PLoS ONE* **2014**, *9*, e109288. [CrossRef] [PubMed]
166. Leal, F.; Nirwan, V.; Gonçalves, A.M.; Panitschewski, N.; Filová, E.; Fahmi, A.; Costa, P.F. Bio-Inspired Nanoporous Scaffold: Electrospun Hybrid Fibers Based on Self-Assembled Block Copolymer Mineralized with Inorganic Nanoparticles for Bone Tissue Engineering. *Int. J. Polym. Mater. Polym. Biomater.* **2023**, *73*, 1054. [CrossRef]
167. Kumar, B.Y.S.; Isloor, A.M.; Kumar, G.C.M.; Inamuddin Asiri, A.M. Nanohydroxyapatite Reinforced Chitosan Composite Hydrogel with Tunable Mechanical and Biological Properties for Cartilage Regeneration. *Sci. Rep.* **2019**, *9*, 15957. [CrossRef] [PubMed]
168. Kumai, T.; Yui, N.; Yatabe, K.; Sasaki, C.; Fujii, R.; Takenaga, M.; Fujiya, H.; Niki, H.; Yudoh, K. A Novel, Self-Assembled Artificial Cartilage-Hydroxyapatite Conjugate for Combined Articular Cartilage and Subchondral Bone Repair: Histopathological Analysis of Cartilage Tissue Engineering in Rat Knee Joints. *Int. J. Nanomed.* **2019**, *14*, 1283. [CrossRef]
169. Boller, L.A.; Shiels, S.M.; Florian, D.C.; Peck, S.H.; Schoenecker, J.G.; Duvall, C.; Wenke, J.C.; Guelcher, S.A. Effects of Nanocrystalline Hydroxyapatite Concentration and Skeletal Site on Bone and Cartilage Formation in Rats. *Acta Biomater.* **2021**, *130*, 485. [CrossRef]
170. Huang, J.; Huang, Z.; Liang, Y.; Yuan, W.; Bian, L.; Duan, L.; Rong, Z.; Xiong, J.; Wang, D.; Xia, J. 3D Printed Gelatin/Hydroxyapatite Scaffolds for Stem Cell Chondrogenic Differentiation and Articular Cartilage Repair. *Biomater. Sci.* **2021**, *9*, 2620. [CrossRef] [PubMed]
171. Gaweł, J.; Milan, J.; Żebrowski, J.; Płoch, D.; Stefaniuk, I.; Kus-Liśkiewicz, M. Biomaterial Composed of Chitosan, Riboflavin, and Hydroxyapatite for Bone Tissue Regeneration. *Sci. Rep.* **2023**, *13*, 17004. [CrossRef]
172. Becerra, J.; Rodriguez, M.; Leal, D.; Noris-Suarez, K.; Gonzalez, G. Chitosan-Collagen-Hydroxyapatite Membranes for Tissue Engineering. *J. Mater. Sci. Mater. Med.* **2022**, *33*, 18. [CrossRef]
173. Ma, S.; Wei, Y.; Sun, R.; Xu, H.; Liu, X.; Wang, Y.; Liang, Z.; Hu, Y.; Lian, X.; Ma, X.; et al. Calcium Phosphate Bone Cements Incorporated with Black Phosphorus Nanosheets Enhanced Osteogenesis. *ACS Biomater. Sci. Eng.* **2023**, *9*, 292. [CrossRef]
174. Witte, F.; Kaese, V.; Haferkamp, H.; Switzer, E.; Meyer-Lindenberg, A.; Wirth, C.J.; Windhagen, H. In vivo Corrosion of Four Magnesium Alloys and the Associated Bone Response. *Biomaterials* **2005**, *26*, 3557. [CrossRef]
175. Liu, C.; Fu, X.; Pan, H.; Wan, P.; Wang, L.; Tan, L.; Wang, K.; Zhao, Y.; Yang, K.; Chu, P.K. Biodegradable Mg-Cu Alloys with Enhanced Osteogenesis, Angiogenesis, and Long-Lasting Antibacterial Effects. *Sci. Rep.* **2016**, *6*, 27374. [CrossRef] [PubMed]
176. Li, R.W.; Kirkland, N.T.; Truong, J.; Wang, J.; Smith, P.N.; Birbilis, N.; Nisbet, D.R. The Influence of Biodegradable Magnesium Alloys on the Osteogenic Differentiation of Human Mesenchymal Stem Cells. *J. Biomed. Mater. Res. A* **2014**, *102*, 4346. [CrossRef] [PubMed]
177. Gonzalez, J.; Hou, R.Q.; Nidadavolu, E.P.S.; Willumeit-Römer, R.; Feyerabend, F. Magnesium Degradation under Physiological Conditions—Best Practice. *Bioact. Mater.* **2018**, *3*, 174. [CrossRef]
178. Fischerauer, S.F.; Kraus, T.; Wu, X.; Tangl, S.; Sorantin, E.; Hänzi, A.C.; Löffler, J.F.; Uggowitzer, P.J.; Weinberg, A.M. In vivo Degradation Performance of Micro-Arc-Oxidized Magnesium Implants: A Micro-CT Study in Rats. *Acta Biomater.* **2013**, *9*, 5411. [CrossRef]

179. Du, L.; Wu, J.; Han, Y.; Wu, C. Immunomodulatory Multicellular Scaffolds For Tendon-to-Bone Regeneration. *Sci. Adv.* **2024**, *10*, eadk6610. [CrossRef]
180. Oliveira-Filho, G.B.; Atoche-Medrano, J.J.; Aragón, F.F.H.; Mantilla Ochoa, J.C.; Pacheco-Salazar, D.G.; da Silva, S.W.; Coaquira, J.A.H. Core-Shell Au/Fe_3O_4 Nanocomposite Synthesized by Thermal Decomposition Method: Structural, Optical, and Magnetic Properties. *Appl. Surf. Sci.* **2021**, *563*, 150290. [CrossRef]
181. Lin, R.H.; Lee, H.T.; Yeh, C.A.; Yang, Y.C.; Shen, C.C.; Chang, K.B.; Liu, B.S.; Hsieh, H.H.; Wang, H.M.; Hung, H.S. Favorable Biological Performance Regarding the Interaction Between Gold Nanoparticles and Mesenchymal Stem Cells. *Int. J. Mol. Sci.* **2022**, *24*, 5. [CrossRef]
182. Hu, X.; Zhang, Y.; Ding, T.; Liu, J.; Zhao, H. Multifunctional Gold Nanoparticles: A Novel Nanomaterial for Various Medical Applications and Biological Activities. *Front. Bioeng. Biotechnol.* **2020**, *8*, 990. [CrossRef]
183. Gupta, R.; Rai, B. Effect of Size and Surface Charge of Gold Nanoparticles on their Skin Permeability: A Molecular Dynamics Study. *Sci. Rep.* **2017**, *7*, 45292. [CrossRef]
184. Suh, K.S.; Lee, Y.S.; Seo, S.H.; Kim, Y.S.; Choi, E.M. Gold Nanoparticles Attenuates Antimycin A-Induced Mitochondrial Dysfunction in MC3T3-E1 Osteoblastic Cells. *Biol. Trace Elem. Res.* **2013**, *153*, 428. [CrossRef]
185. Grant, S.A.; Zhu, J.; Gootee, J.; Snider, C.L.; Bellrichard, M.; Grant, D.A. Gold Nanoparticle-Collagen Gels for Soft Tissue Augmentation. *Tissue Eng. Part A* **2018**, *24*, 1091. [CrossRef] [PubMed]
186. Nunan, R.; Harding, K.G.; Martin, P. Clinical Challenges of Chronic Wounds: Searching for an Optimal Animal Model to Recapitulate their Complexity. *Dis. Model Mech.* **2014**, *7*, 1205. [CrossRef] [PubMed]
187. Mendes, C.; Thirupathi, A.; Zaccaron, R.P.; Corrêa, M.E.; Bittencourt, J.V.; Casagrande, L.D.; de Lima, A.C.; de Oliveira, L.L.; de Andrade, T.A.; Gu, Y.; et al. Microcurrent and Gold Nanoparticles Combined with Hyaluronic Acid Accelerates Wound Healing. *Antioxidants* **2022**, *11*, 2257. [CrossRef]
188. Poomrattanangoon, S.; Pissuwan, D. Gold Nanoparticles Coated with Collagen-I and Their Wound Healing Activity in Human Skin Fibroblast Cells. *Heliyon* **2024**, *10*, e33302. [CrossRef] [PubMed]
189. Ibrahim, B.; Akere, T.H.; Chakraborty, S.; Valsami-Jones, E.; Ali-Boucetta, H. Gold Nanoparticles Induced Size Dependent Cytotoxicity on Human Alveolar Adenocarcinoma Cells by Inhibiting the Ubiquitin Proteasome System. *Pharmaceutics* **2023**, *15*, 432. [CrossRef]
190. Zhang, X.D.; Wu, D.; Shen, X.; Liu, P.X.; Yang, N.; Zhao, B.; Zhang, H.; Sun, Y.M.; Zhang, L.A.; Fan, F.Y. Size-Dependent in vivo Toxicity of PEG-Coated Gold Nanoparticles. *Int. J. Nanomed.* **2011**, *6*, 2071. [CrossRef]
191. Surapaneni, S.K.; Bashir, S.; Tikoo, K. Gold Nanoparticles-Induced Cytotoxicity in Triple Negative Breast Cancer Involves Different Epigenetic Alterations Depending upon the Surface Charge. *Sci. Rep.* **2018**, *8*, 12295. [CrossRef]
192. Paramasivam, V.; Paulpandian, P.; Venkatachalam, K.; Hussain, S.; Kangal, A.; Al Farraj, D.A.; Elshikh, M.S.; Balaji, P. Cytotoxicity and Antimicrobial Efficiency of Gold (Au) Nanoparticles Formulated by Green Approach using Andrographis Paniculata Leaf Extract. *J. King Saud. Univ. Sci.* **2023**, *35*, 102687. [CrossRef]
193. Bertsch, C.; Maréchal, H.; Gribova, V.; Lévy, B.; Debry, C.; Lavalle, P.; Fath, L. Biomimetic Bilayered Scaffolds for Tissue Engineering: From Current Design Strategies to Medical Applications. *Adv. Healthc. Mater.* **2023**, *12*, e2203115. [CrossRef]
194. Del Bakhshayesh, A.R.; Asadi, N.; Alihemmati, A.; Tayefi Nasrabadi, H.; Montaseri, A.; Davaran, S.; Saghati, S.; Akbarzadeh, A.; Abedelahi, A. An Overview of Advanced Biocompatible and Biomimetic Materials for Creation of Replacement Structures in the Musculoskeletal Systems: Focusing on Cartilage Tissue Engineering. *J. Biol. Eng.* **2019**, *13*, 85. [CrossRef]
195. Patterson, J.; Martino, M.M.; Hubbell, J.A. Biomimetic Materials in Tissue Engineering. *Mater. Today* **2010**, *13*, 14. [CrossRef]
196. Liu, S.; Yu, J.M.; Gan, Y.C.; Qiu, X.Z.; Gao, Z.C.; Wang, H.; Chen, S.X.; Xiong, Y.; Liu, G.H.; Lin, S.E.; et al. Bioomimetic Natural Biomaterials For Tissue Engineering and Regenerative Medicine: New Biosynthesis Methods, Recent Advances, and Emerging Applications. *Mil. Med. Res.* **2023**, *10*, 16. [CrossRef]
197. Ma, P.X. Biomimetic Materials for Tissue Engineering. *Adv. Drug Deliv. Rev.* **2008**, *60*, 184. [CrossRef] [PubMed]
198. Qin, L.; Yang, S.; Zhao, C.; Yang, J.; Li, F.; Xu, Z.; Yang, Y.; Zhou, H.; Li, K.; Xiong, C.; et al. Prospects and Challenges For the Application of Tissue Engineering Technologies in the Treatment of Bone Infections. *Bone Res.* **2024**, *12*, 28. [CrossRef]
199. Senra, M.R.; Marques, M.F.V.; Monteiro, S.N. Poly (Ether-Ether-Ketone) For Biomedical Applications: From Enhancing Bioactivity to Reinforced-Bioactive Composites-An Overview. *Polymers* **2023**, *15*, 373. [CrossRef] [PubMed]
200. Cao, D.; Ding, J. Recent Advances in Regenerative Biomaterials. *Regen. Biomater.* **2022**, *9*, rbac098. [CrossRef]
201. Sun, Y.; Liu, X.; Tan, J.; Lv, D.; Song, W.; Su, R.; Li, L.; Liu, X.; Ouyang, L.; Liao, Y. Strontium Ranelate Incorporated 3D Porous Sulfonated PEEK Simulating MC3T3-E1 Cell Differentiation. *Regen. Biomater.* **2020**, *8*, rbaa043. [CrossRef]
202. Vasconcelos, D.P.; Águas, A.P.; Barbosa, M.A.; Pelegrín, P.; Barbosa, J.N. The Inflammasome in Host Response to Biomaterials: Bridging Inflammation and Tissue Regeneration. *Acta Biomater.* **2019**, *83*, 1. [CrossRef]
203. Lele, M.; Kapur, S.; Hargett, S.; Sureshbabu, N.M.; Gaharwar, A.K. Global Trends in Clinical Trials Involving Engineered Biomaterials. *Sci. Adv.* **2024**, *10*, eabq0997. [CrossRef]
204. Elson, E.L.; Genin, G.M. Tissue Constructs: Platforms for Basic Research and Drug Discovery. *Interface Focus* **2016**, *6*, 20150095. [CrossRef]
205. Hench, L.L.; Thompson, I. Twenty-First Century Challenges for Biomaterials. *J. R. Soc. Interface* **2010**, *7*, S379. [CrossRef] [PubMed]
206. Sharma, P.; Kumar, P.; Sharma, R.; Bhatt, V.D.; Dhot, P.S. Tissue Engineering; Current Status & Futuristic Scope. *J. Med. Life* **2019**, *12*, 225. [CrossRef] [PubMed]

207. Chandra, P.K.; Soker, S.; Atala, A. Chapter 1—Tissue Engineering: Current Status and Future Perspectives. In *Principles of Tissue Engineering*, 5th ed.; Lanza, R., Langer, R., Vacanti, J.P., Atala, A., Eds.; Academic Press: London, UK, 2020; pp. 1–35.
208. Ashammakhi, N.; GhavamiNejad, A.; Tutar, R.; Fricker, A.; Roy, I.; Chatzistavrou, X.; Hoque Apu, E.; Nguyen, K.L.; Ahsan, T.; Pountos, I.; et al. Highlights on Advancing Frontiers in Tissue Engineering. *Tissue Eng. Part B Rev.* **2022**, *28*, 633. [CrossRef] [PubMed]
209. Badylak, S.F.; Nerem, R.M. Progress in Tissue Engineering and Regenerative Medicine. *Proc. Natl. Acad. Sci. USA* **2010**, *107*, 3285. [CrossRef] [PubMed]

Disclaimer/Publisher's Note: The statements, opinions and data contained in all publications are solely those of the individual author(s) and contributor(s) and not of MDPI and/or the editor(s). MDPI and/or the editor(s) disclaim responsibility for any injury to people or property resulting from any ideas, methods, instructions or products referred to in the content.